Article

Molecular Cell

A Cancer-Specific Ubiquitin Ligase Drives mRNA Alternative Polyadenylation by Ubiquitinating the mRNA 3′ End Processing Complex

Graphical Abstract

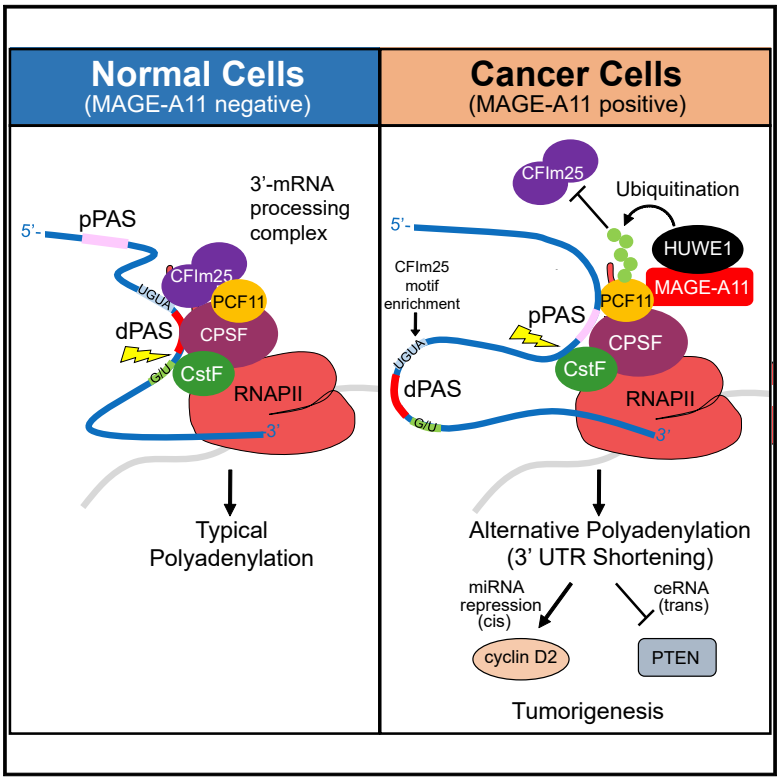

Highlights

- MAGE-A11 is aberrantly expressed in cancer and is a potent oncogene
- MAGE-A11-HUWE1 ubiquitin ligase promotes ubiquitination and degradation of PCF11
- MAGE-A11 promotes alternative polyadenylation and 3′ UTR shortening in cancer
- MAGE-A11-induced 3′ UTR shortening modulates core oncogenes and tumor suppressors

Authors

Seung Wook Yang, Lei Li, Jon P. Connelly, ..., Shondra M. Pruett-Miller, Wei Li, Patrick Ryan Potts

Correspondence

ryan.potts@stjude.org

In Brief

Yang et al. show that the germ-cell-restricted MAGE-A11 is aberrantly expressed in tumors and drives tumorigenesis through ubiquitination of PCF11, a component of the 3′-mRNA processing complex. PCF11 ubiquitination results in alternative polyadenylation of transcripts leading to 3′ UTR shortening.

Yang et al., 2020, Molecular Cell 77, 1206–1221
March 19, 2020
https://doi.org/10.1016/j.molcel.2019.12.022

CellPress

CellPress

Molecular Cell
Article

A Cancer-Specific Ubiquitin Ligase Drives mRNA Alternative Polyadenylation by Ubiquitinating the mRNA 3′ End Processing Complex

Seung Wook Yang,[1,6] Lei Li,[2,3,6] Jon P. Connelly,[1] Shaina N. Porter,[1] Kiran Kodali,[4] Haiyun Gan,[1] Jung Mi Park,[1] Klementina Fon Tacer,[1] Heather Tillman,[5] Junmin Peng,[4] Shondra M. Pruett-Miller,[1] Wei Li,[2,3] and Patrick Ryan Potts[1,7,*]

[1]Department of Cell and Molecular Biology, St. Jude Children's Research Hospital, Memphis, TN 38105, USA
[2]Department of Biological Chemistry, School of Medicine, University of California, Irvine, Irvine, CA 92697, USA
[3]Division of Biostatistics, Dan L. Duncan Cancer Center and Department of Molecular and Cellular Biology, Baylor College of Medicine, Houston, TX 77030, USA
[4]Departments of Structural Biology and Developmental Neurobiology, Center for Proteomics and Metabolomics, St. Jude Children's Research Hospital, Memphis, TN 38105, USA
[5]Veterinary Pathology Core, St. Jude Children's Research Hospital, Memphis, TN 38105, USA
[6]These authors contributed equally
[7]Lead Contact
*Correspondence: ryan.potts@stjude.org
https://doi.org/10.1016/j.molcel.2019.12.022

SUMMARY

Alternative polyadenylation (APA) contributes to transcriptome complexity by generating mRNA isoforms with varying 3′ UTR lengths. APA leading to 3′ UTR shortening (3′ US) is a common feature of most cancer cells; however, the molecular mechanisms are not understood. Here, we describe a widespread mechanism promoting 3′ US in cancer through ubiquitination of the mRNA 3′ end processing complex protein, PCF11, by the cancer-specific MAGE-A11–HUWE1 ubiquitin ligase. MAGE-A11 is normally expressed only in the male germline but is frequently re-activated in cancers. MAGE-A11 is necessary for cancer cell viability and is sufficient to drive tumorigenesis. Screening for targets of MAGE-A11 revealed that it ubiquitinates PCF11, resulting in loss of CFIm25 from the mRNA 3′ end processing complex. This leads to APA of many transcripts affecting core oncogenic and tumor suppressors, including cyclin D2 and PTEN. These findings provide insights into the molecular mechanisms driving APA in cancer and suggest therapeutic strategies.

INTRODUCTION

Alternative polyadenylation (APA) of messenger RNA (mRNA) is a widespread phenomenon that frequently occurs in a large proportion of human genes (Elkon et al., 2013; Ji et al., 2009; Mayr and Bartel, 2009; Sandberg et al., 2008). Recent studies have shown that at least 70% of mammalian genes have multiple polyadenylation sites (PASs) in their 3′ untranslated regions (UTRs) (Derti et al., 2012; Hoque et al., 2013). Selection of the PAS is coordinated by recognition of core sequence elements in the mRNA by the mRNA 3′ end processing complex that is composed of several protein complexes, including CPSF, CFI, CFII, and CstF complexes, and single proteins, such as PABPN1, RBBP6, and SYMPK (Elkon et al., 2013; Shi et al., 2009; Tian and Manley, 2017). Modulation of components of these complexes can lead to the use of cryptic PASs, resulting in APA (Martin et al., 2012; Masamha et al., 2014; Yao et al., 2012).

The consequences of APA can be significant, with effects on post-transcriptional gene regulation, including mRNA stability, translation, nuclear export, and cellular localization (reviewed in Tian and Manley, 2017). One well-noted consequence of APA resulting in 3′ UTR shortening (3′ US) is mRNA evasion of microRNA (miRNA)-based repression (Hoffman et al., 2016; Mayr and Bartel, 2009; Sandberg et al., 2008). In addition to regulating cognate transcripts in *cis*, 3′ US can lead to competing-endogenous RNA (ceRNA) regulation in *trans* such that the shortened 3′ UTRs no longer sequester miRNAs and the released miRNAs can be directed to repress their ceRNA partners (Salmena et al., 2011).

APA can be a regulated process that is required for normal physiological functions, including cellular differentiation, neuronal activity, and spermatogenesis (Flavell et al., 2008; Ji and Tian, 2009; Li et al., 2016). For example, APA leading to 3′ UTR lengthening of transcripts in the brain is frequent and results in diverse protein isoforms with differential subcellular localization (Ciolli Mattioli et al., 2019; Miura et al., 2013). Furthermore, 3′ US is associated with T lymphocyte activation and induced proliferation (Sandberg et al., 2008), as well as male germ cell differentiation (MacDonald and Redondo, 2002).

Aberrant APA is often associated with disease, including in cancer, where global 3′ US is a hallmark of most tumors (Fu et al., 2011; Masamha et al., 2014; Mayr and Bartel, 2009; Xia et al., 2014). Pan-cancer analysis revealed that >90% of APA events lead to 3′ US (Xia et al., 2014). Several oncogenes are known to be affected, including the cyclin D1 cell cycle regulator,

whose levels are increased due to 3′ US (Mayr and Bartel, 2009). Our recent study also suggests that 3′ US in breast cancer can repress tumor suppressor genes in *trans* by disrupting ceRNA crosstalk (Park et al., 2018). Despite these observations, the mechanisms that promote APA are not well established. Although 3′ US in a subset of glioblastomas can be attributed to CFIm25 downregulation (Masamha et al., 2014), the genetic underpinnings for the vast majority of tumors is largely unknown.

MAGE genes are conserved in all eukaryotes and are defined by a common MAGE homology domain (MHD), which consists of tandem winged helix motifs (Doyle et al., 2010; Lee and Potts, 2017; Newman et al., 2016). A subset of human MAGE proteins is categorized as cancer-testis antigens (CTAs) because they are physiologically restricted to the testis but are aberrantly expressed in cancers (Pineda et al., 2015; Simpson et al., 2005). Recently, MAGE CTAs have gained growing interest as hallmarks of cancers because of their broad expression in aggressive cancers, correlation with poor clinical prognosis, and their oncogenic ability to promote increased tumor growth and metastasis (Pineda et al., 2015; Weon and Potts, 2015). We and others have shown that MAGE proteins function as substrate adaptors through their ability to recruit novel proteins to specific E3 ubiquitin ligases to promote their ubiquitination and often degradation (Doyle et al., 2010; Hao et al., 2013; Pineda et al., 2015). Thus, MAGE proteins may represent a way in which tumors co-opt germ cell functions to rewire key signaling pathways in cancer cells by reprogramming ubiquitin ligases. However, the molecular mechanisms and oncogenic potential of most MAGE CTAs, including MAGE-A11, are unknown.

Here, we show that the normally germ-cell-restricted MAGE-A11 is aberrantly expressed in cancer and acts as a potent oncogene that drives tumorigenesis by promoting APA leading 3′ US of many transcripts. MAGE-A11 acts as a substrate adaptor for the HUWE1 E3 ubiquitin ligase to promote aberrant ubiquitination of the PCF11 subunit of the mRNA 3′ end processing complex in cancer cells. This leads to the loss of CFIm25 from the mRNA 3′ end processing complex and results in 3′ US of transcripts that have enrichment of CFIm25 binding sites upstream of their distal PASs. Importantly, expression of a non-degradable PCF11 mutant suppressed MAGE-A11 oncogenic activity and 3′ US. Analysis of the transcripts affected by MAGE-A11 revealed core oncogenic and tumor suppressor genes and pathways. This includes 3′ US of the cyclin D2 oncogene leading to deregulation of the Rb tumor suppressor pathway. Furthermore, ceRNA partners of 3′ US transcripts included many tumor suppressor genes, such as PTEN that is downregulated by MAGE-A11, resulting in activation of the Akt growth signaling pathway. These findings provide insights into the function of MAGE-A11 and help explain the molecular mechanisms driving APA in cancer.

RESULTS

MAGE-A11 Is Aberrantly Expressed in Cancer and Is Necessary and Sufficient to Drive Tumor Growth

To thoroughly examine the expression pattern of *MAGE-A11*, we analyzed its expression by qRT-PCR in 26 disease-free human tissues and found that it is normally restricted to expression in the testis and placenta (Figure 1A). These findings were confirmed in 51 human tissues from the GTEx project (Figure S1A) and at the protein level by immunohistochemistry, showing expression of MAGE-A11 in germ cells of the testis and syncytiotrophoblasts in placental tissue (Figures S1B and S1C). Like other CTA genes, MAGE-A11 is aberrantly expressed in tumors (Bai et al., 2005; Lian et al., 2012; Su et al., 2013; Xia et al., 2013). Our analysis of The Cancer Genome Atlas (TCGA) transcriptomic data revealed that *MAGE-A11* is frequently expressed in many patient tumors, including lung squamous cell carcinoma (>60%), ovarian carcinoma (>40%), and head and neck squamous cell carcinoma (>40%) (Figure 1B). Furthermore, immunohistochemistry staining of ovarian carcinoma and lung squamous cell carcinoma tumor microarrays confirmed MAGE-A11 protein (Figures S1D and S1E) in 35% of samples (n = 211), regardless of tumor stage or grade (Figure S1F).

To determine whether the aberrant expression of MAGE-A11 in tumor cells is simply a passenger event due to global genomic dysregulation or whether MAGE-A11 has a more active role in driving tumorigenesis, we performed a series of gain- and loss-of-function studies to elucidate the role of MAGE-A11 in driving cancer cell growth. First, we examined whether multiple cancer cells require the expression of MAGE-A11 for viability. Intriguingly, transient knockdown of MAGE-A11 in H520 lung squamous cell carcinoma cells and DAOY medulloblastoma cells resulted in dramatic decrease in cell viability (Figure 1C). Furthermore, knockout of MAGE-A11 decreased the proliferation rate of DAOY and H520 cells, which could be rescued by re-expression of MAGE-A11 (Figures 1D and S1G–S1I). Furthermore, knockout of MAGE-A11 reduced other hallmarks of cancer, such as clonogenic growth and anchorage-independent growth of H520 and DAOY cells (Figures 1E–1G, S1J, and S1K). Re-expression of MAGE-A11 rescued anchorage-independent tumor growth (Figure 1G). Consistent with these findings, knockout of MAGE-A11 slowed xenograft tumor growth, and re-expression of MAGE-A11 rescued tumor growth in mice (Figures 1H and S2A–S2E). Finally, to determine whether overexpression of MAGE-A11 is sufficient to drive tumorigenic phenotypes, we stably expressed MAGE-A11 in A2780 or OV56 ovarian cancer cells that do not naturally express MAGE-A11. Strikingly, expression of MAGE-A11 accelerated anchorage-independent growth of A2780 cells (Figure S2F) and xenograft tumor growth of A2780 and OV56 cells in mice (Figures 1I, 1J, S2G, and S2H). Together, these results suggest that MAGE-A11 is normally restricted to expression in the testis and placenta but is aberrantly expressed in a variety of cancers, where it is necessary and sufficient to drive tumorigenesis.

MAGE-A11 Promotes Ubiquitination and Proteasome-Dependent Degradation of PCF11

To elucidate the molecular mechanisms of MAGE-A11 oncogenic activity, we performed unbiased analysis of MAGE-A11 interacting proteins by tandem affinity purification (TAP) coupled to liquid chromatography-tandem mass spectrometry (LC-MS/MS). Only 4 proteins, PCF11, CLP1, POLR2A, and POLR2B, in addition to the MAGE-A11 bait, were identified repeatedly and specifically in TAP-MAGE-A11 cells compared to TAP-vector controls (Figures 2A and S3A). Remarkably, all four proteins

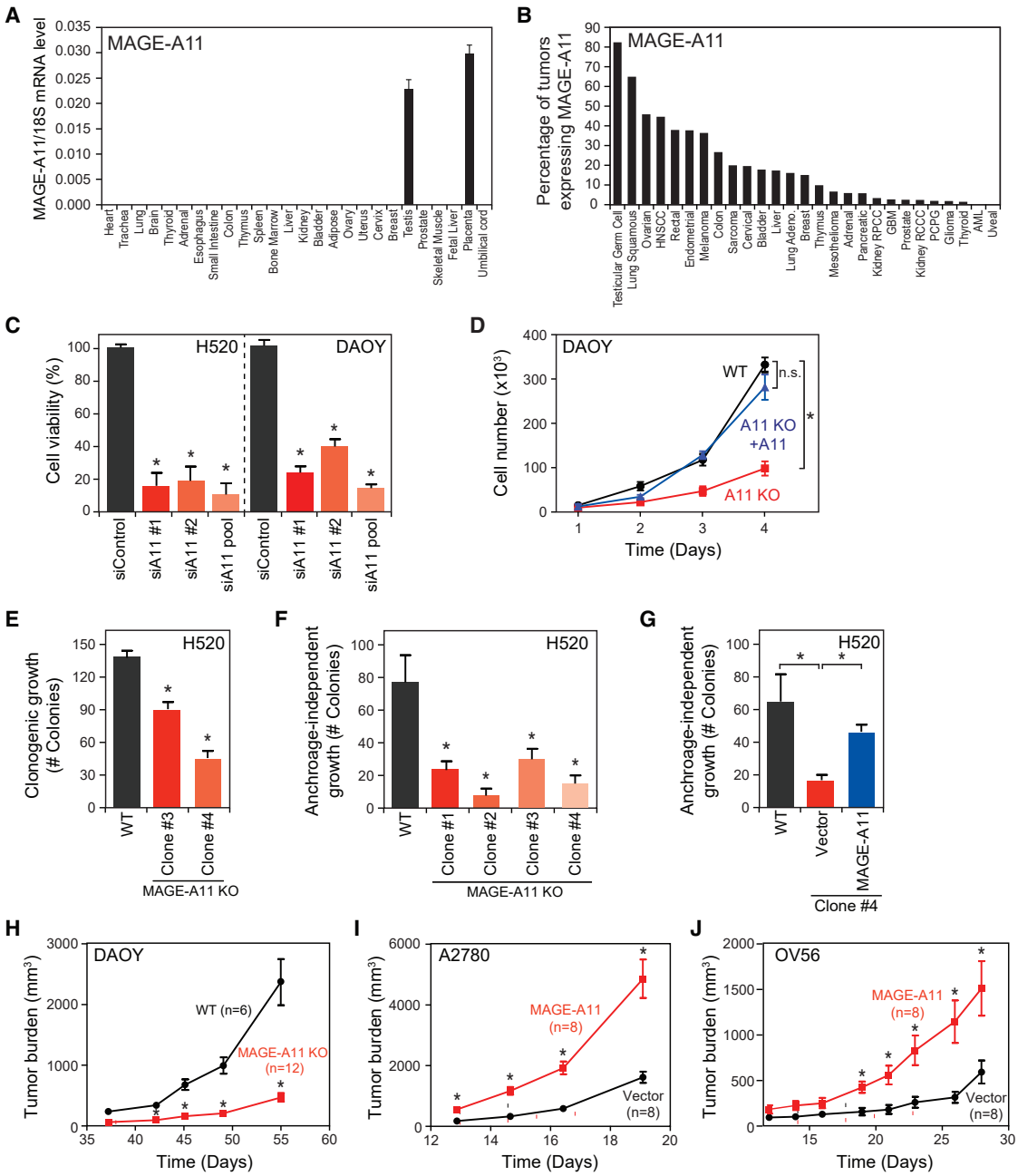

Figure 1. MAGE-A11 Is Aberrantly Expressed in Cancer and Is Necessary and Sufficient to Drive Tumor Growth

(A) qRT-PCR analysis of the normalized expression of human *MAGE-A11* in the indicated tissues (n = 3).

(B) Percentage of patient tumors expressing *MAGE-A11* is shown.

(C) H520 lung squamous cell carcinoma cells and DAOY cerebellar medulloblastoma cells were transfected with control, MAGE-A11 no. 1, MAGE-A11 no. 2, or MAGE-A11 pool siRNAs, and cell viability was measured by alamarBlue assay 72 h later.

(D) MAGE-A11-knockout DAOY cells or those reconstituted with MAGE-A11 were counted for cell proliferation at the indicated time points.

(E and F) Wild-type H520 cells or MAGE-A11-knockout H520 clones were assayed for clonogenic growth (E) and for anchorage-independent growth in soft agar colony formation assays (F).

(G) Re-expression of MAGE-A11 rescues anchorage-independent growth of MAGE-A11-knockout H520 cells.

(H) Knockout of MAGE-A11 in DAOY decreases xenograft tumor growth in mice (n = 6 for wild-type group; n = 12 for MAGE-A11-knockout group).

(I and J) Stable expression of MAGE-A11 in MAGE-A11-negative A2780 (I) and OV56 (J) ovarian cancer cells increases xenograft tumor growth in mice (n = 8 per group). Data are mean ± SD. *p < 0.05.

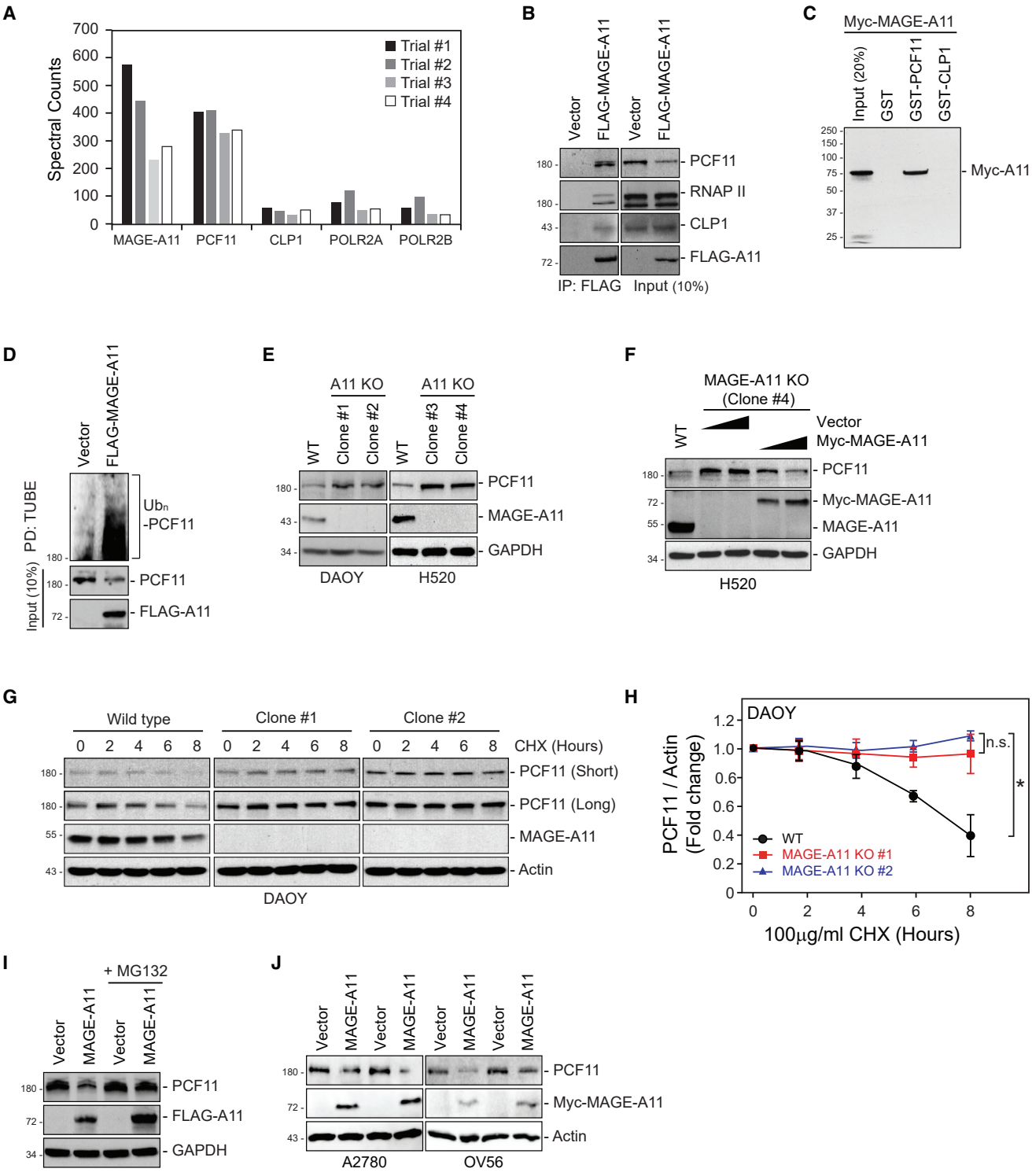

Figure 2. MAGE-A11 Promotes Ubiquitination and Degradation of PCF11

(A) MAGE-A11 interacts with 3′ mRNA processing complex proteins. HEK293 cells stably expressing TAP-vector or TAP-MAGE-A11 were subjected to pull-down followed by SDS-PAGE and LC-MS/MS (n = 4). Note spectral counts for all indicated proteins were 0 in TAP-vector samples.

(B) Interaction between MAGE-A11 and 3′ mRNA processing proteins were validated by immunoprecipitation (IP). HEK293FT cells stably expressing FLAG-vector or FLAG-MAGE-A11 were subjected to pull-down with anti-FLAG followed by SDS-PAGE and immunoblotting for endogenous PCF11, RNAP II, and CLP1.

(C) Recombinant glutathione S-transferase (GST)-PCF11, but not GST-CLP1, binds *in vitro* translated Myc-MAGE-A11.

(legend continued on next page)

are known to interact within the context of the mRNA 3′ end processing complex. PCF11 and CLP1 belong to the cleavage factor II (CFII) subcomplex that directly interacts with RNA polymerase II (RNAPII) via p-S2 residues in the RNAPII CTD-binding PCF11 CID domain (Licatalosi et al., 2002; Meinhart and Cramer, 2004). We confirmed that MAGE-A11 interacts with the CFII complex and RNAPII in cells by co-immunoprecipitation (coIP) (Figure 2B). Further analysis revealed that the MAGE-A11 directly binds PCF11, but not CLP1 (Figure 2C), *in vitro*.

Previously, we have reported that many MAGE proteins bind to specific E3 ubiquitin ligases and modulate ubiquitination of target proteins (Doyle et al., 2010; Hao et al., 2013, 2015; Pineda et al., 2015; Weon et al., 2018). Consistent with this, we found that MAGE-A11 increased PCF11 ubiquitination (Figure 2D). Knockout of MAGE-A11 increased PCF11 protein levels in DAOY and H520 cells (Figure 2E) that could be rescued by re-expression of MAGE-A11 (Figures 2F and S3B). These results were confirmed by protein half-life measurements that showed increased stability of PCF11 in MAGE-A11 knockout cells (Figures 2G and 2H). Furthermore, MAGE-A11 overexpression decreased PCF11 levels in A2780, OV56, and HEK293FT cells in a proteasome-dependent manner (Figures 2I and 2J). Importantly, this effect was specific to PCF11, as MAGE-A11 expression did not alter levels of CPSF, CstF, and CFI complexes or PCF11-interacting proteins (Figure S3C).

MAGE-A11 Recruits PCF11 to the HUWE1 E3 Ubiquitin Ligase for Ubiquitination and Degradation

Next, we utilized the previously described ubiquitin-activated interaction trap (UBAIT) approach (O'Connor et al., 2015) to identify which E3 ubiquitin ligase partners with MAGE-A11 to promote PCF11 ubiquitination and degradation. Follow-up analysis of the candidate E3 ligases revealed that HUWE1 is required for the MAGE-A11-mediated ubiquitination and degradation of PCF11. We confirmed that MAGE-A11 interacted with HUWE1 (Figure 3A) and recruited PCF11 to the HUWE1 ligase (Figure 3B), consistent with the function of MAGEs as substrate adapters. Depletion of MAGE-A11 or HUWE1 decreased ubiquitination of PCF11 (Figure 3C) and increased PCF11 protein levels (Figure 3D). Furthermore, MAGE-A11 induced PCF11 degradation in a HUWE1-dependent manner (Figure 3E). These results were confirmed by protein half-life measurements that showed increased stability of PCF11 upon HUWE1 knockdown in DAOY cells naturally expressing MAGE-A11 (Figure 3F). Together, these results suggest that MAGE-A11 targets PCF11 for ubiquitination and degradation by the HUWE1 E3 ubiquitin ligase.

MAGE-A11 Promotes Alternative Polyadenylation Leading to 3′ US in Tumors

Because PCF11 is one of the polyA cleavage factors responsible for mRNA 3′ end processing, we examined whether MAGE-A11 regulation of PCF11 would alter PAS choice, leading to APA and changes in 3′ UTR length. We performed high-depth (2.5×10^8 reads) RNA sequencing (RNA-seq) and applied our previously described bioinformatics algorithm DaPars (dynamic analysis of alternative polyadenylation from RNA-seq) (Masamha et al., 2014; Xia et al., 2014) to identify 3′ UTR alterations between control and MAGE-A11-expressing HEK293FT cells. The difference in 3′ UTR length between samples was quantified as a change in percentage of distal PAS usage index (PDUI). MAGE-A11 expression resulted in 268 APA events, with the majority, 213, being 3′ US events in which the proximal PAS (pPAS) was preferentially used (Figures 4A and 4B). Similar results were also obtained using the APAtrap algorithm (Ye et al., 2018) with a large number of 3′ US transcripts identified by both approaches (χ^2 $p < 0.00001$). In contrast to MAGE-A11 expression, knockout of MAGE-A11 in DAOY cells resulted in significantly more transcripts with 3′ UTR lengthening ($p = 0.008254$; Figure S4A). These results suggest that MAGE-A11 promotes 3′ US of transcripts.

Next, to examine whether MAGE-A11 induces 3′ US in tumors, we analyzed APA events in A2780 and OV56 xenograft tumors from mice. We identified 531 and 275 significant APA events driven by MAGE-A11 in OV56 and A2780 tumors, respectively (Figures 4C–4E). These APA events were almost exclusively 3′ US (95% and 84% of APA events in OV56 and A2780 tumors, respectively; Figures 4C and 4D). This included a statistically enriched ($p = 1.01^{-8}$) core set of common 3′ US transcripts altered in each tumor type, with a large number of cell-type-specific 3′ US transcripts. Furthermore, analysis of TCGA transcriptomics datasets from human ovarian carcinoma and lung squamous carcinoma patient tumors for 3′ UTR usage revealed a significant number of transcripts (106 [85% of APA events] and 151 [87% of APA events], respectively) with 3′ US in MAGE-A11-expressing tumors compared to MAGE-A11-negative control tumors (Figures 4F–4H). Notably, many of the transcripts with APA had altered mRNA levels, consistent with disruption of *cis*-regulatory elements in the 3′ UTR of these transcripts (Figures S4B–S4F). Together, these results suggest that MAGE-A11 regulation of PCF11 drives APA leading to 3′ US in tumors.

MAGE-A11-Induced PCF11 Ubiquitination Dissociates CFIm25 from RNAPII

Previous studies have shown that changes in the levels of specific components of the mRNA 3′ end processing complex can

(D) Expression of MAGE-A11 promotes PCF11 ubiquitination. Ubiquitinated proteins from FLAG-vector or FLAG-MAGE-A11 stably expressing HEK293FT cells were isolated with tandem ubiquitin binding entity (TUBE)-agarose followed by SDS-PAGE and immunoblotting for endogenous PCF11.

(E) Knockout of MAGE-A11 increases PCF11 protein levels. Wild-type or MAGE-A11 knockout DAOY or H520 cells were blotted for the indicated proteins.

(F) Re-expression of MAGE-A11 decreases PCF11 protein levels in MAGE-A11 knockout H520 cells. Increasing amounts of MAGE-A11 were stably expressed in MAGE-A11 knockout-H520 cells.

(G and H) Knockout of MAGE-A11 increases PCF11 protein stability in DAOY cells. MAGE-A11 wild-type or knockout DAOY cells were treated with 100 μg/mL cycloheximide for the indicated times. Cell lysates were immunoblotted (G) and quantitated (H; n = 3). Data are mean ± SD. *$p < 0.05$.

(I) MAGE-A11 promotes proteasome-dependent PCF11 degradation. HEK293FT cells stably expressing FLAG-vector or FLAG-MAGE-A11 were treated with 10 μM MG132 for 4 h before immunoblotting.

(J) Stable expression of MAGE-A11 decreases PCF11 protein levels in A2780 and OV56 cells. Cell lysates were blotted for the indicated proteins.

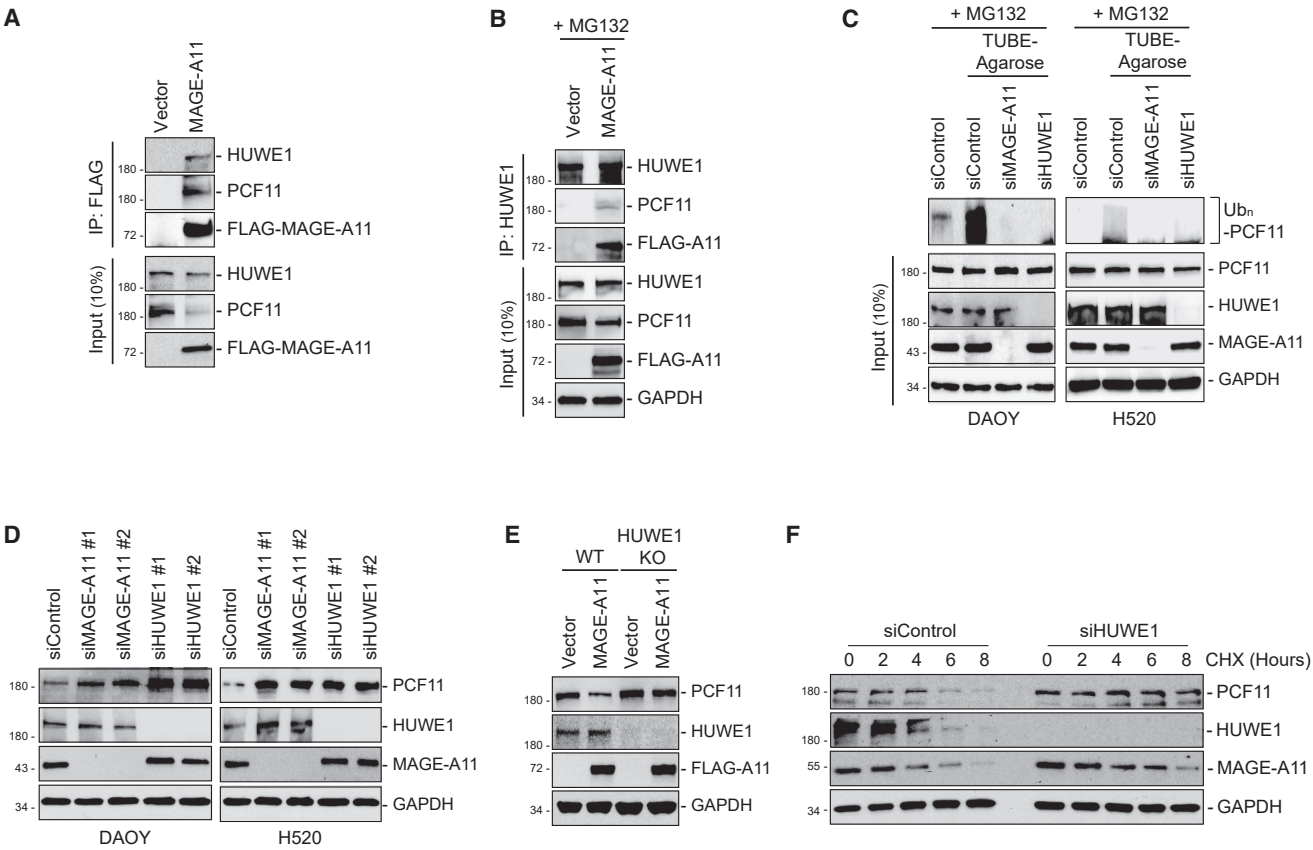

Figure 3. MAGE-A11 Recruits PCF11 to the HUWE1 E3 Ubiquitin Ligase for Ubiquitination and Degradation

(A) MAGE-A11 interacts with PCF11 and HUWE1. HEK293FT cells stably expressing FLAG-vector or FLAG-MAGE-A11 were subjected to pull-down with anti-FLAG followed by SDS-PAGE and immunoblotting for anti-HUWE1 and anti-PCF11.

(B) MAGE-A11 promotes PCF11 binding to HUWE1 E3 ubiquitin ligase. HEK293FT cells stably expressing FLAG-vector or FLAG-MAGE-A11 were treated with 10 μM MG132 for 4 h followed by IP with anti-HUWE1, SDS-PAGE, and immunoblotting for the indicated proteins.

(C) MAGE-A11-induced ubiquitination of PCF11 depends on HUWE1 E3 ligase. DAOY or H520 cells were transfected with the indicated siRNAs for 72 h and treated with 10 μM MG132 for 4 h followed by pull-down with TUBE-agarose, SDS-PAGE, and immunoblotting for PCF11.

(D) Depletion of MAGE-A11 or HUWE1 increases PCF11 protein levels. DAOY or H520 cells were transfected with the indicated siRNAs for 72 h and blotted for the indicated proteins.

(E) MAGE-A11-induced PCF11 degradation is dependent on HUWE1. Wild-type or HUWE1 knockout HEK293T cells stably expressing FLAG-vector or FLAG-MAGE-A11 were immunoblotted for the indicated proteins.

(F) Knockdown of HUWE1 increases PCF11 protein stability in DAOY cells that express MAGE-A11. siControl or siHUWE1 DAOY cells were treated with 100 μg/mL cycloheximide for the indicated times. Cell lysates were immunoblotted for the indicated proteins.

lead to APA. Although depletion of CFIm25 by small interfering RNA (siRNA)-mediated knockdown led to 3′ US, depletion of PCF11 produced 3′ UTR lengthening (Baejen et al., 2017; Kamieniarz-Gdula et al., 2019; Li et al., 2015; Masamha et al., 2014; Ogorodnikov et al., 2018). In contrast, our data suggest that MAGE-A11-induced PCF11 ubiquitination leads to 3′ US (Figure 4). Importantly, there was very little overlap (10 transcripts) in MAGE-A11-indued 3′ US transcripts (213 transcripts) and PCF11 siRNA-induced 3′ UTR lengthened transcripts (545 transcripts), suggesting that dynamic MAGE-A11-induced ubiquitination of PCF11 has distinct outcomes compared to static siRNA-mediated knockdown of PCF11. To explore this further, we examined whether MAGE-A11 ubiquitination of PCF11 could alter the architecture of the mRNA 3′ end processing complex. We found that MAGE-A11 expression resulted in significant reduction in CFIm25 association with RNAPII by coIP (Figures 5A, 5B, and S5A). Moreover, this effect was more pronounced in comparison to siRNA-mediated knockdown of PCF11 (Figures 5A, 5B, and S5A). Consistent with these findings, there is significant overlap (42%; $p = 7.8^{-55}$) in the 3′ US transcripts upon CFIm25 knockdown in HeLa cells (Masamha et al., 2014) and MAGE-A11 overexpression in HEK293FT cells (Figure S5B). Next, we determined whether ubiquitination and/or degradation of PCF11 are required for MAGE-A11-induced CFIm25 dissociation from RNAPII. CFIm25 dissociation from RNAPII by MAGE-A11 is HUWE1 dependent, confirming the importance of ubiquitination (Figure 5C). However, this effect was independent of PCF11 degradation, as rescue of PCF11 levels in MAGE-A11-expressing cells by MG132 led to stabilization of PCF11 but failed to rescue CFIm25 association with RNAPII

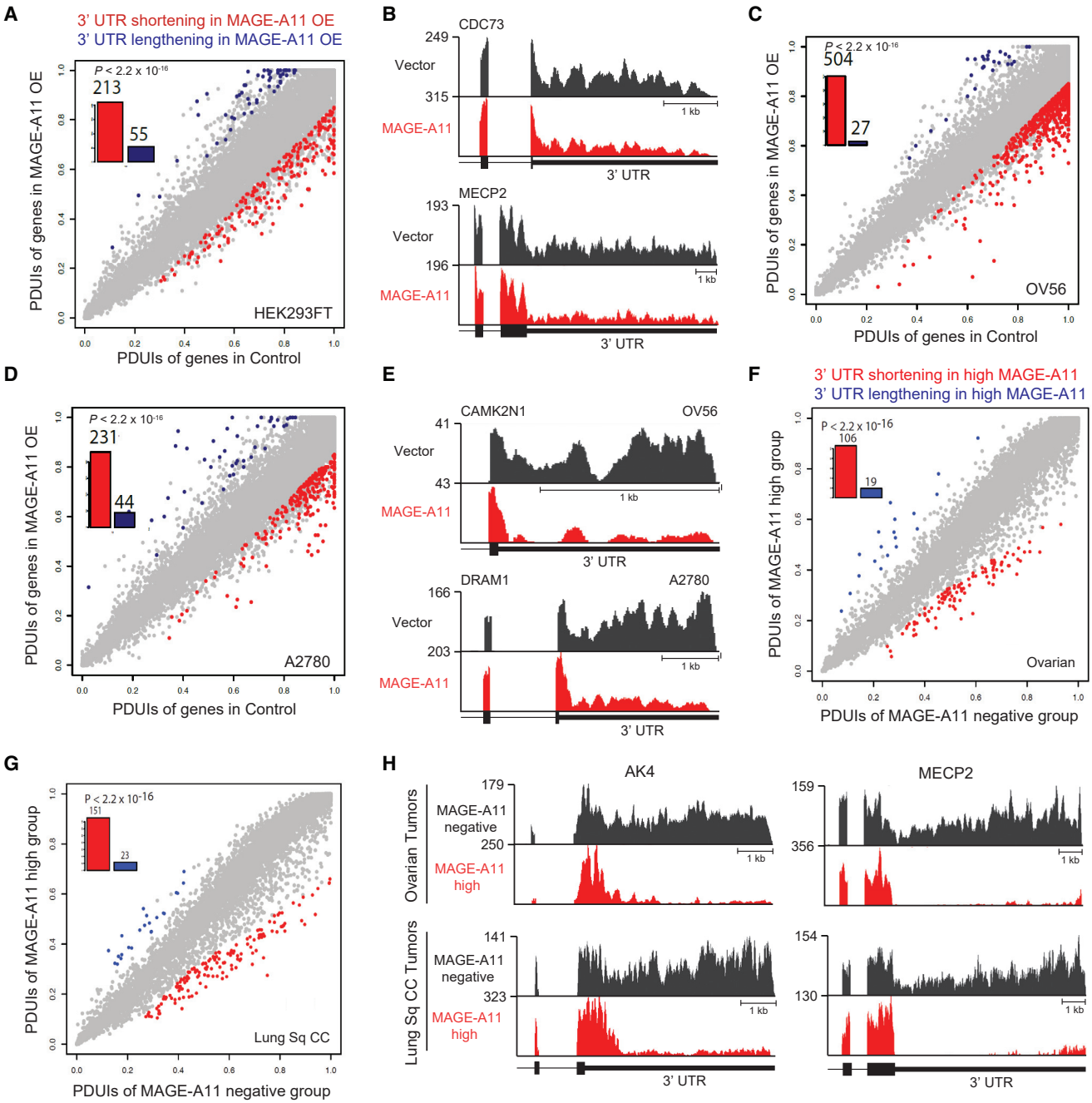

Figure 4. MAGE-A11 Promotes Alternative Polyadenylation Leading to 3′ UTR Shortening in Tumors

(A) Transcriptome analysis of HEK293FT cells stably expressing FLAG-vector or FLAG-MAGE-A11 reveals that MAGE-A11 promotes 3′ US. Scatterplot of percentage of distal polyA site usage index (PDUI) in control and MAGE-A11-overexpressing cells shows shortened 3′ UTRs (n = 213) or lengthened 3′ UTRs (n = 55) in genes by overexpression of MAGE-A11. False discovery rate (FDR) ≤ 0.05, ΔPDUIs ≥ 0.2 and 2-fold change of PDUIs between control and MAGE-A11 overexpression are colored. The shifting toward pPAS is significant ($p < 2.2 \times 10^{-16}$; binomial test).

(B) Representative RNA-seq density plots for genes with 3′ UTR shortening are shown. Numbers on y axis indicate RNA-seq read coverage.

(C and D) Scatterplot of PDUIs from both datasets of mouse xenografts in Figures 1I and 1J using the same cutoffs as in (A). Data from OV56 and A2780 tumors are shown in (C) and (D), respectively. The shifting toward pPAS is significant ($p < 2.2 \times 10^{-16}$; binomial test).

(E) Representative examples of genes with 3′ UTR shortening from datasets shown in (C) and (D) are shown.

(F and G) Global analysis of 3′ UTR changes in ovarian cancer (F) or lung squamous cell carcinoma (G) patient samples with either negative or high levels of MAGE-A11. Scatterplot of PDUIs from both datasets of patient samples is shown. The shifting toward pPAS is significant ($p < 2.2 \times 10^{-16}$; binomial test).

(H) Representative examples of genes show 3′ UTR shortening in patient samples with negative (black) or high MAGE-A11 expression levels (red).

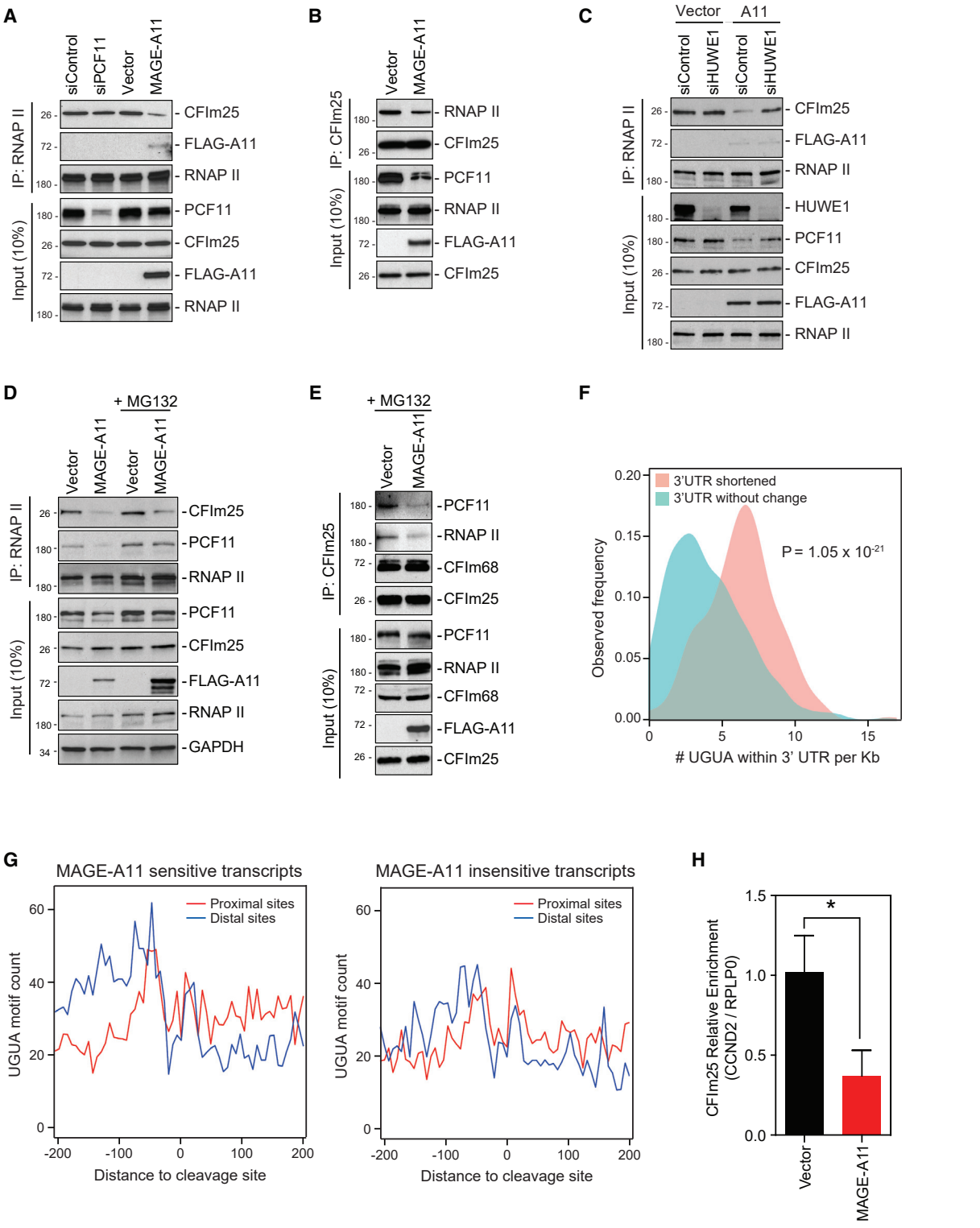

Figure 5. MAGE-A11-Induced PCF11 Ubiquitination Dissociates CFIm25 from RNAPII

(A and B) Overexpression of MAGE-A11 induces dissociation of CFIm25 from RNAPII compared to knockdown of PCF11. HEK293FT cells were transfected with the indicated siRNAs for 72 h or stably expressing FLAG-vector or FLAG-MAGE-A11 were followed by IP with anti-RNAPII (A) and IP with anti-CFIm25 (B), SDS-PAGE, and immunoblotting for the indicated proteins.

(legend continued on next page)

(Figures 5D and 5E). Notably, PCF11 interaction with RNAPII was not altered by MAGE-A11 in MG132-treated cells (Figure 5D). These results suggest that MAGE-A11-induced PCF11 ubiquitination, but not degradation, causes remodeling of the mRNA 3′ end processing complex that leads to dissociation of CFIm25. Moreover, simple steady-state depletion of PCF11 by siRNA does not mimic the effect of MAGE-A11-induced ubiquitination of PCF11.

Consistent with the dissociation of CFIm25 from RNAPII playing an important role in MAGE-A11-induced 3′ US, sequence analysis of MAGE-A11-sensitive transcripts revealed significantly more CFIm25 binding motifs (UGUA) compared to unaffected transcripts (Figure 5F). Furthermore, analysis of UGUA motif distribution near distal and proximal PASs, as described previously (Zhu et al., 2018), showed motif enrichment upstream of distal PASs in MAGE-A11-sensitive transcripts, but not proximal PASs or transcripts unaffected by MAGE-A11 (Figures 5G and S5C–S5F). This was not the case for transcripts lengthened by PCF11 siRNA-mediated knockdown (Figures S5G and S5H). Collectively, these findings provide insights into how PCF11 ubiquitination affects the mRNA 3′ end processing complex through loss of CFIm25 that leads to 3′ US of transcripts with enriched UGUA motifs upstream distal PASs. To further test this model, we performed crosslinking immunoprecipitation and qPCR (CLIP-qPCR) to determine the abundance of CFIm25 associated with a transcript, *CCND2*, which undergoes 3′ US upon MAGE-A11 expression. Expression of MAGE-A11 significantly reduced the abundance of CFIm25 associated with the *CCND2* transcript in relation to a non-MAGE-A11-regulated transcript, RPLP0 (Figure 5H).

Regulation of PCF11 Is Essential for MAGE-A11-Induced Tumorigenesis and APA

To determine whether regulation of PCF11 is required for MAGE-A11 oncogenic activity, we identified a non-degradable PCF11 mutant. The degron motif in PCF11 required for MAGE-A11 binding was mapped to amino acids 653–702 (Figures 6A, 6B, and S6A–S6D). Mutation of conserved residues in PCF11 (Figure S6E) identified I689A mutant that abolished PCF11 interaction with MAGE-A11 (Figures 6C and S6F) and disrupted ubiquitination and degradation by MAGE-A11 (Figure 6D). Importantly, introduction of PCF11 I689A into A2780 cells, by a transgene or homozygous mutation using CRISPR/Cas9, rescued PCF11 protein levels (Figures 6E and 6G) and completely or partially (depending on the clone) blocked MAGE-A11-induced xenograft tumor growth in mice (Figures 6F, 6H, S6G, and S6H). Importantly, MAGE-A11-driven APA was dependent on its regulation of PCF11, as expression of the non-degradable PCF11 I689A mutant by transgene or CRISPR/Cas9 homozygous knockin prevented MAGE-A11-induced APA in A2780 cells (Figures 6I, 6J, and S6I). These results suggest that the ability of MAGE-A11 to regulate PCF11 is critical for its oncogenic activity.

MAGE-A11-Induced 3′ US Modulates Core Oncogenic and Tumor Suppressor Pathways

To identify those 3′ US events that impact levels of their encoded proteins, we performed unbiased, quantitative proteomics using tandem mass tagging (TMT)-LC/LC-MS/MS (Niu et al., 2017) in isogenic DAOY cells with or without MAGE-A11 expression (Table S3). Consistent with previous results, PCF11 was downregulated upon MAGE-A11 expression (Figure 7A). More importantly, we found several 3′ US transcripts with altered protein levels, including the *CCND2* (cyclin D2) oncogene that was upregulated upon MAGE-A11 expression (Figure 7A). We validated these results by expressing MAGE-A11 in an independent cell line, HEK293FT, and again saw 3′ US of the *CCND2* transcript (Figures 7B and S7A) and increased protein levels (Figures 7C and 7D). As a member of the D-type cyclins, cyclin D2 has been widely implicated in cell cycle transition, differentiation, and cellular transformation (Evron et al., 2001; Sherr, 1995), and its overexpression is highly correlated with poor prognosis in various cancers (Mermelshtein et al., 2005; Sicinski et al., 1996; Takano et al., 1999, 2000). Cyclin D-Cdk4/6 inactivates retinoblastoma (Rb) tumor suppressor by progressive multi-phosphorylation to release transcription factors, such as E2F (Narasimha et al., 2014; Sherr, 1995). MAGE-A11 increased phospho-Rb (S807 and S811) in HEK293FT cells and MAGE-A11 expression in ovarian and lung squamous cell carcinoma patient tumor samples correlated with increased phospho-Rb (S807/811; Figures 7E, 7F, and S7B). To determine whether cyclin D2 upregulation upon MAGE-A11 expression contributes to MAGE-A11-driven proliferation, cyclin D2 was knocked down in DAOY cells with or without MAGE-A11 expression and proliferation rates were determined. Knockdown of cyclin D2 decreased proliferation of MAGE-A11 expressing DAOY, but not MAGE-A11 knockout DAOY (Figure 7G), thus implicating upregulation of cyclin D2 by MAGE-A11 as an important contributor to MAGE-A11-mediated cellular proliferation.

To better understand how *CCND2* 3′ US may upregulate cyclin D2 protein levels, we determined whether inhibitory factors, such

(C) HUWE1 is required for MAGE-A11-induced dissociation of CFIm25 from RNAPII. HEK293FT FLAG-vector or FLAG-MAGE-A11 stable cell lines were transfected with the indicated siRNAs for 72 h followed by IP with anti-RNAPII, SDS-PAGE, and immunoblotting for the indicated proteins.

(D) PCF11 ubiquitination, but not degradation, promotes CFIm25 dissociation from RNAPII. HEK293 FLAG-vector or FLAG-MAGE-A11 stable cell lines were treated with or without 10 μM MG132 for 4 h prior to collection, anti-RNAPII IP, SDS-PAGE, and immunoblotting.

(E) MAGE-A11 dissociates CFIm25 from PCF11. Cells were treated as described in (D) before IP with anti-CFIm25, SDS-PAGE, and immunoblotting for the indicated proteins.

(F) The number of UGUA motifs within 3′ US or unaffected transcripts in MAGE-A11 overexpressing HEK293FT cells. Equal numbers of transcripts with no 3′ UTR changes were randomly selected.

(G) The UGUA motif frequency within MAGE-A11-sensitive transcripts is highly enriched upstream of distal PAS compared to proximal PAS (ΔPDUI value $\leq$ 0.05; $p > 0.5$) for 3′ US transcripts, but not MAGE-A11-insensitive transcripts.

(H) MAGE-A11 reduces CFIm25 associated with 3′ US transcript *CCND2*. CLIP-qPCR analysis was performed from HEK293FT cells using control immunoglobulin G (IgG) or CFIm25 antibodies. Abundance of CCND2 or control RPLP0 was determined by qRT-PCR. Normalized (CFIm25/IgG) ratios of CCND2 and RPLP0 are shown. Data (n = 3) are mean ± SD. *$p < 0.05$.

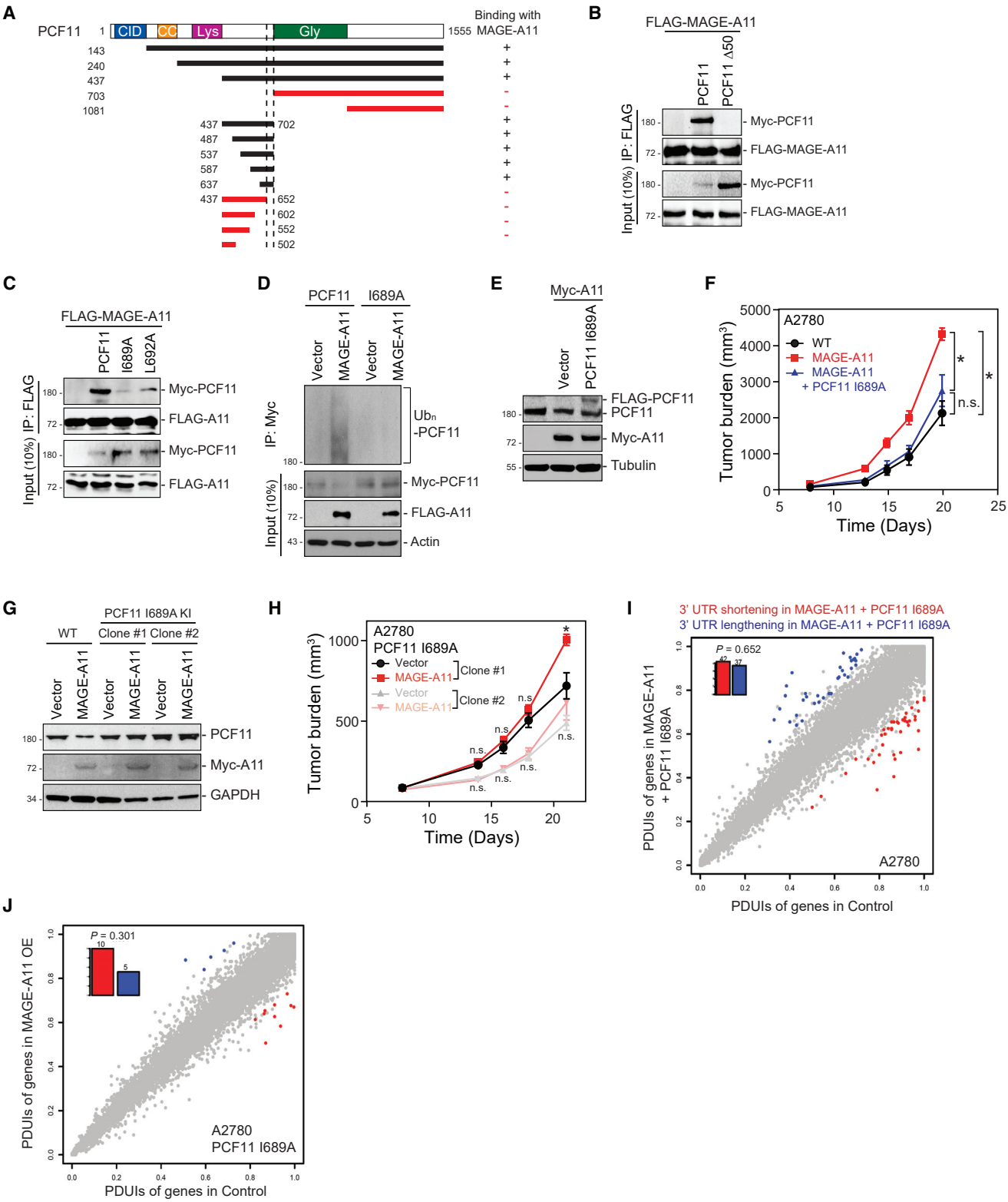

(legend on next page)

as miRNAs, may repress cyclin D2 expression in MAGE-A11-negative HEK293FT cells. We used the approach pioneered by others to overexpress the 3′ UTR of *CCND2* to act as a ''sponge'' for potential miRNAs and other factors binding to the endogenous *CCND2* transcript (Mallon and Macklin, 2002; Matoulkova et al., 2012; Rutnam and Yang, 2012). We found that expression of the *CCND2* 3′ UTR upregulated cyclin D2 protein levels in MAGE-A11-negative, but not MAGE-A11-positive, cells (Figures 7H and S7C). In order to determine which particular miRNA(s) might mediate cyclin D2 repression, we analyzed the predicted miRNA binding sites (TargetScan; Agarwal et al., 2015) lost upon *CCND2* 3′ US and correlated these to miRNA expression datasets (miRmine; Panwar et al., 2017) to identify relevant miRNAs. Using this approach, we identified miR-191-5p, a previously reported miRNA targeting *CCND2* (Di Leva et al., 2013), as a likely candidate. We found that the miR-191-5p mimic downregulated cyclin D2 protein levels and miR-191-5p antagomiR increased cyclin D2 protein levels in MAGE-A11-negative cells, but not in MAGE-A11 expressing cells (Figures 7I and 7J). These results suggest that MAGE-A11-mediated 3′ US of *CCND2* leads to increased cyclin D2 protein levels, in part through loss of miR-191-5p repression.

In addition to 3′ US of oncogenes leading to their activation in *cis* through evading miRNA-mediated repression, we and others have also shown that these now-liberated miRNAs can downregulate competing endogenous mRNAs (ceRNAs) in *trans* (Park et al., 2018). Using our previously established computational approach to predict the *trans* effect of 3′ US to their ceRNA partners (Park et al., 2018), we found that many 3′ US ceRNA partners in ovarian cancer or lung squamous cell carcinoma patient samples with high MAGE-A11 levels are tumor suppressors (Figure 7K). Notably, the top ceRNA identified in MAGE-A11 lung squamous cell carcinoma was the tumor suppressor PTEN (Table S4). Consistently, MAGE-A11 expression markedly downregulated PTEN levels and increased downstream phospho-AKT (T308) in HEK293FT cells (Figures 7L and S7D) and ovarian carcinoma patient tumor samples (Figure 7M). To determine whether this effect depends on miRNA targeting of the *PTEN* 3′ UTR, we utilized a luciferase reporter plasmid containing the *PTEN* 3′ UTR. MAGE-A11 expression repressed *PTEN* 3′ UTR luciferase activity (Figure S7E). These results suggest that MAGE-A11-induced 3′ US has both *cis* and *trans* effects on oncogenes (cyclin D2) and tumor suppressors (PTEN), respectively, to alter key cell growth and signaling pathways.

DISCUSSION

The eukaryotic mRNA 3′ end processing complex plays an essential role in defining the transcriptome. This molecular machine interacts with the transcription machinery to define mRNA termination through cleavage of pre-mRNA and polyA tail addition. Recent transcriptomic studies have shown that a majority of mammalian genes have multiple PASs and APA contributes to the complexity of the transcriptome by generating mRNA isoforms with varying 3′ UTR lengths (Derti et al., 2012; Mayr and Bartel, 2009; Sandberg et al., 2008). Interestingly, widespread shortening of mRNA by APA is found in many types of cancers, but the molecular mechanisms contributing to APA in cancer have been unclear. Our findings elucidate a previously undefined molecular mechanism contributing to the widespread 3′ US in tumors.

The regulation of PCF11 ubiquitination by the cancer-specific E3 ubiquitin ligase MAGE-A11–HUWE1 led to changes in the mRNA 3′ end processing complex and increased the number of 3′ US transcripts in cancers. Interestingly, PCF11 is a sub-stoichiometric component of the mRNA 3′ end processing complex in many human cells and tissues (Kamieniarz-Gdula et al., 2019). Thus, even small fluctuations in PCF11 may impact mRNA 3′ end processing and the dynamics of PCF11 association with the mRNA 3′ end processing complex may be important. This is consistent with our findings that MAGE-A11-induced ubiquitination of PCF11 confers unique phenotypes compared to steady-state siRNA knockdown of PCF11. Furthermore, PCF11 couples mRNA 3′ end processing with mRNA export (Johnson et al., 2009) and phosphorylation of PCF11 CID by WNK1 is critical for release of transcripts from chromatin-associated RNAPII (Volanakis et al., 2017). Therefore, nuclear export of mature transcripts in tumor cells could potentially be regulated by MAGE-A11-mediated PCF11 ubiquitination.

Analysis of the transcripts affected by MAGE-A11-induced ubiquitination of PCF11 revealed many oncogenes and tumor suppressors. First, we and others have shown that 3′ US of oncogenes results in their increased production through evading miRNA-mediated repression. Indeed, the alternative isoforms, especially shorter transcripts of genes encoding cyclin D1, cyclin

Figure 6. Regulation of PCF11 Is Essential for MAGE-A11-Induced Tumorigenesis and APA

(A) Summary of *in vitro* binding assays from Figures S6A–S6C mapping the degron region of PCF11 recognized by MAGE-A11.

(B) HEK293FT cells stably expressing FLAG-MAGE-A11 were transfected with PCF11 wild-type or PCF11 653–702 deletion construct for 48 h before IP with anti-FLAG followed by SDS-PAGE and immunoblotting for anti-Myc.

(C) PCF11 I689A or L692A mutants have diminished interaction with MAGE-A11. HEK293FT cells stably expressing FLAG-MAGE-A11 were transfected with the indicated constructs for 48 h before IP with anti-FLAG followed by SDS-PAGE and immunoblotting for anti-Myc.

(D) PCF11 I689A mutant fails to be ubiquitinated and degraded by MAGE-A11. HEK293FT cells stably expressing FLAG-vector or FLAG-MAGE-A11 were transfected with indicated constructs for 48 h before IP with anti-Myc followed by SDS-PAGE and immunoblotting for anti-His.

(E and F) Non-degradable PCF11 I689A was stably expressed in MAGE-A11-expressing A2780 (E), and xenograft tumor growth was determined (F). Data are mean ± SD (n = 6 per group). *p < 0.05.

(G) CRISPR-Cas9-mediated knockin of non-degradable PCF11 I689A mutant into A2780 prevents degradation of PCF11 by MAGE-A11.

(H) Stable expression of MAGE-A11 in PCF11 I689A knockin A2780 clones does not increase xenograft tumor growth in mice (n = 6 per group). Data are mean ± SD. *p < 0.05.

(I and J) Expression (I) or knockin (J) of non-degradable PCF11 I689A rescues 3′ US in A2780 MAGE-A11-expressing tumors. Scatterplot of PDUIs (as described in Figure 4A) from mouse xenografts shown in (F) or (H) is shown. The pPAS is not significant (p = 0.652, I; p = 0.301, J; binomial test).

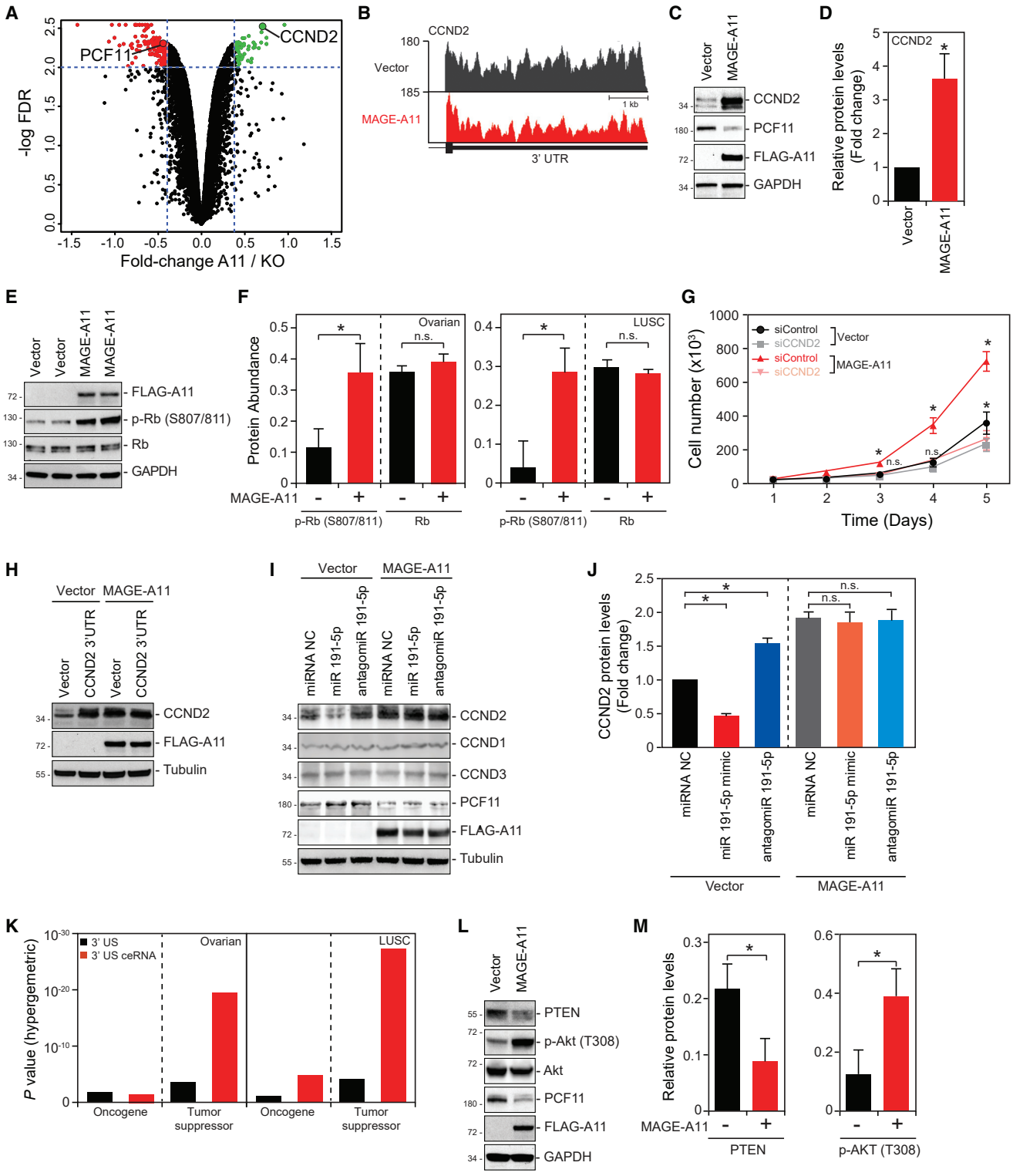

Figure 7. MAGE-A11-Induced 3′ UTR Shortening Modulates Oncogenes and Tumor Suppressors

(A) Quantitative whole-cell proteomics using TMT labeling (n = 5) revealed upregulation of CCND2 (cyclin D2) oncogene upon MAGE-A11 expression in DAOY MAGE-A11 KO cells.

(B) RNA-seq tracks for CCND2 showing reduced 3′ UTR reads in MAGE-A11-expressing cells.

(legend continued on next page)

D2, and FGF2, are more prominently detected in cancers compared to normal tissues (Mayr and Bartel, 2009). Furthermore, 3′ US of cyclin D1 in lymphomas correlates with increased cyclin D1 expression and proliferation of the lymphoma cells (Rosenwald et al., 2003). Interestingly, we found that MAGE-A11 induced 3′ US of cyclin D2, but not cyclin D1 or cyclin D3, resulting in increased protein products (Figures 7C, 7D, and 7I). These results suggest that MAGE-A11 may selectively regulate gene expression through modulation of APA leading to 3′ US in cancers. Second, we report that 3′ US possesses a significant role as ceRNAs for tumor-suppressor genes in *trans* (Park et al., 2018). Intriguingly, the ceRNA partners of 3′ US genes upon expression of MAGE-A11 are strongly enriched for tumor suppressors in lung squamous cell carcinoma ($p = 1.93^{-26}$) and ovarian cancer ($p = 7.71^{-21}$). Remarkably, these are notable tumor suppressors, such as PTEN, whose downregulation resulted in upregulation of Akt pro-survival signaling. These findings indicate MAGE-A11 may orchestrate gene expression changes in *cis* and in *trans* by modulating APA that results in reprogramming critical cellular signaling pathways, such as cell cycle and Akt signaling, to drive tumorigenesis. These findings may have important implications on therapeutic strategies for treating cancer, as MAGE-A11 expression status may confer predictive power to the response of cells against therapies, such as CDK4/6 inhibitors and AKT pathway inhibitors.

APA is known to be differentially regulated across tissue types and developmental stages such that an APA signature, ratio of distal versus proximal PAS choice, can be found. For example, compared to mammalian somatic cells, male germ cells have remarkable APA leading to 3′ US of many transcripts. In particular, PAS choice in male germ cells is often unique compared to somatic cells and results in testis-specific transcripts (Li et al., 2016; MacDonald, 2019; MacDonald and Redondo, 2002). It is not fully appreciated what leads to the widespread alternative PAS usage in germ cells leading to 3′ US but has been suggested to involve changes in the composition of the polyadenylation machinery, including CFIm (Edwalds-Gilbert et al., 1997; McMahon et al., 2006; Sartini et al., 2008; Takagaki and Manley, 1998). Our findings suggest that MAGE-A11–HUWE1 may be important factors in promoting APA in male germ cells. Consistently, HUWE1 has been shown to be important for spermatogonial differentiation and entry into meiosis (Bose et al., 2017). Furthermore, we suggest that the ability of MAGE-A11 to induce APA in cancer cells is not a neomorphic activity but rather is a conserved function of MAGE-A11 in cancer and germ cells.

Overall, our results suggest that dynamic regulation of the mRNA 3′ end processing machinery by ubiquitination can serve as a mechanism to control APA in various biological and pathological states.

STAR★METHODS

Detailed methods are provided in the online version of this paper and include the following:

- KEY RESOURCES TABLE
- LEAD CONTACT AND MATERIALS AVAILABILITY
- EXPERIMENTAL MODEL AND SUBJECT DETAILS
  - Animals
  - Cell lines
  - Microbe strains
- METHOD DETAILS
  - Cell culture transfections
  - Generation of stable overexpression cell lines
  - siRNA and miRNAs
  - Tandem affinity purification
  - RNA preparation and quantitative reverse transcription PCR Analysis (qRT-PCR)
  - Clonogenic growth and anchorage-independent growth soft agar assays
  - Immunoprecipitation and immunoblotting
  - Recombinant protein purification and *in vitro* binding assay
  - Tandem ubiquitin binding entity (TUBE) ubiquitination assay
  - Cell viability assay
  - Xenograft tumor growth assays
  - LightSwitch luciferase reporter assay
  - RNA-seq
  - CRISPR/Cas9 genome editing
  - TCGA 3′-UTR analysis

(C and D) MAGE-A11 overexpression increases cyclin D2 protein levels. HEK293FT cells stably expressing FLAG-vector or FLAG-MAGE-A11 were immunoblotted for the indicated proteins (C) and quantitated (D). Data are mean ± SD (n = 3). *p < 0.05.

(E and F) MAGE-A11 induces phosphorylation of retinoblastoma (Rb). HEK293FT cells stably expressing FLAG-vector or FLAG-MAGE-A11 were immunoblotted for the indicated proteins (E), and ovarian cancer or lung squamous cell carcinoma patient samples with either low or high levels of MAGE-A11 were analyzed for phospho-Rb (S807/811) and total Rb protein levels (F). Data are mean ± SE of tumors indicated. *p < 0.01.

(G) Depletion of CCND2 decreases the proliferation rate of MAGE-A11-re-expressing DAOY cells. MAGE-A11-knockout DAOY cells or those reconstituted with MAGE-A11 were transfected with the indicated siRNAs for 48 h counted for cell proliferation at the indicated time points. Data are mean ± SD. *p < 0.05.

(H) *CCND2* 3′ UTR upregulates CCND2 in HEK293FT control cells, but not those stably expressing MAGE-A11. The indicated HEK293FT cells were transfected with vector control or *CCND2* 3′ UTR for 48 h and blotted for the indicated proteins.

(I and J) miR191-5p decreases CCND2 expression. HEK293FT cells stably expressing FLAG-vector or FLAG-MAGE-A11 were transfected with indicated miRNAs for 72 h, blotted for the indicated proteins (I), and quantitated (J). Data are mean ± SD (n = 3). *p < 0.05.

(K) Oncogene or tumor suppressor gene enrichment of 3′ US mRNAs and 3′ US competing endogenous RNAs (ceRNAs) in ovarian cancer or lung squamous cell carcinoma patient samples with high MAGE-A11 expression levels. Top 10 tumors as high MAGE-A11 expression levels in two cancer types were analyzed; averaged p values with SD are plotted.

(L and M) MAGE-A11 represses PTEN protein levels through 3′ US in *trans*. HEK293FT cells stably expressing FLAG-vector or FLAG-MAGE-A11 were immunoblotted for the indicated proteins (L), and patient samples with either low (n = 101) or high levels of MAGE-A11 (n = 75) were analyzed for PTEN and phospho-Akt (T308) protein levels (M). Data are mean ± SE of tumors indicated. *p < 0.01.

SUPPLEMENTAL INFORMATION

Supplemental Information can be found online at https://doi.org/10.1016/j.molcel.2019.12.022.

ACKNOWLEDGMENTS

We thank members of the Potts lab for helpful discussions and critical reading of the manuscript. We would also like to thank Dr. George-Lucian Moldovan, Pennsylvania State University College of Medicine, for generously providing HEK293T HUWE1 knockout cells. This work was partially supported by a Worldwide Cancer Research grant 15-0177 (P.R.P.), American Cancer Society Research Scholar Award 181691010 (P.R.P.), and NIH R01 CA193466 (W.L.).

AUTHOR CONTRIBUTIONS

P.R.P. and S.W.Y. conceptualized the study and designed experiments. L.L. and W.L. designed the computational analyses. L.L., W.L., and H.G. analyzed RNA-seq data. K.K. and J.P. performed proteomics. K.F.T. and H.T. performed tissue gene expression and IHC analysis. S.N.P., J.P.C., and S.M.P.-M. performed gene editing. S.W.Y., J.M.P., and P.R.P. performed experiments and analyzed data. S.W.Y. and P.R.P. wrote the manuscript.

DECLARATION OF INTERESTS

The authors declare no competing interests.

Received: September 13, 2019
Revised: December 2, 2019
Accepted: December 23, 2019
Published: January 21, 2020

REFERENCES

Agarwal, V., Bell, G.W., Nam, J.W., and Bartel, D.P. (2015). Predicting effective microRNA target sites in mammalian mRNAs. eLife *4*, e05005.

Anders, S., and Huber, W. (2010). Differential expression analysis for sequence count data. Genome Biol. *11*, R106.

Anders, S., Pyl, P.T., and Huber, W. (2015). HTSeq–a Python framework to work with high-throughput sequencing data. Bioinformatics *31*, 166–169.

Baejen, C., Andreani, J., Torkler, P., Battaglia, S., Schwalb, B., Lidschreiber, M., Maier, K.C., Boltendahl, A., Rus, P., Esslinger, S., et al. (2017). Genome-wide analysis of RNA polymerase II termination at protein-coding genes. Mol. Cell *66*, 38–49.e6.

Bai, S., He, B., and Wilson, E.M. (2005). Melanoma antigen gene protein MAGE-11 regulates androgen receptor function by modulating the interdomain interaction. Mol. Cell. Biol. *25*, 1238–1257.

Bai, B., Tan, H., Pagala, V.R., High, A.A., Ichhaporia, V.P., Hendershot, L., and Peng, J. (2017). Deep profiling of proteome and phosphoproteome by isobaric labeling, extensive liquid chromatography, and mass spectrometry. Methods Enzymol. *585*, 377–395.

Bose, R., Sheng, K., Moawad, A.R., Manku, G., O'Flaherty, C., Taketo, T., Culty, M., Fok, K.L., and Wing, S.S. (2017). Ubiquitin ligase Huwe1 modulates spermatogenesis by regulating spermatogonial differentiation and entry into meiosis. Sci. Rep. *7*, 17759.

Choe, K.N., Nicolae, C.M., Constantin, D., Imamura Kawasawa, Y., Delgado-Diaz, M.R., De, S., Freire, R., Smits, V.A., and Moldovan, G.L. (2016). HUWE1 interacts with PCNA to alleviate replication stress. EMBO Rep. *17*, 874–886.

Ciolli Mattioli, C., Rom, A., Franke, V., Imami, K., Arrey, G., Terne, M., Woehler, A., Akalin, A., Ulitsky, I., and Chekulaeva, M. (2019). Alternative 3′ UTRs direct localization of functionally diverse protein isoforms in neuronal compartments. Nucleic Acids Res. *47*, 2560–2573.

Connelly, J.P., and Pruett-Miller, S.M. (2019). CRIS.py: a versatile and high-throughput analysis program for CRISPR-based genome editing. Sci. Rep. *9*, 4194.

Davoli, T., Xu, A.W., Mengwasser, K.E., Sack, L.M., Yoon, J.C., Park, P.J., and Elledge, S.J. (2013). Cumulative haploinsufficiency and triplosensitivity drive aneuploidy patterns and shape the cancer genome. Cell *155*, 948–962.

Derti, A., Garrett-Engele, P., Macisaac, K.D., Stevens, R.C., Sriram, S., Chen, R., Rohl, C.A., Johnson, J.M., and Babak, T. (2012). A quantitative atlas of polyadenylation in five mammals. Genome Res. *22*, 1173–1183.

Di Leva, G., Piovan, C., Gasparini, P., Ngankeu, A., Taccioli, C., Briskin, D., Cheung, D.G., Bolon, B., Anderlucci, L., Alder, H., et al. (2013). Estrogen mediated-activation of miR-191/425 cluster modulates tumorigenicity of breast cancer cells depending on estrogen receptor status. PLoS Genet. *9*, e1003311.

Dobin, A., Davis, C.A., Schlesinger, F., Drenkow, J., Zaleski, C., Jha, S., Batut, P., Chaisson, M., and Gingeras, T.R. (2013). STAR: ultrafast universal RNA-seq aligner. Bioinformatics *29*, 15–21.

Doyle, J.M., Gao, J., Wang, J., Yang, M., and Potts, P.R. (2010). MAGE-RING protein complexes comprise a family of E3 ubiquitin ligases. Mol. Cell *39*, 963–974.

Edwalds-Gilbert, G., Veraldi, K.L., and Milcarek, C. (1997). Alternative poly(A) site selection in complex transcription units: means to an end? Nucleic Acids Res. *25*, 2547–2561.

Elkon, R., Ugalde, A.P., and Agami, R. (2013). Alternative cleavage and polyadenylation: extent, regulation and function. Nat. Rev. Genet. *14*, 496–506.

Evron, E., Umbricht, C.B., Korz, D., Raman, V., Loeb, D.M., Niranjan, B., Buluwela, L., Weitzman, S.A., Marks, J., and Sukumar, S. (2001). Loss of cyclin D2 expression in the majority of breast cancers is associated with promoter hypermethylation. Cancer Res. *61*, 2782–2787.

Feng, X., Li, L., Wagner, E.J., and Li, W. (2018). TC3A: The Cancer 3′ UTR Atlas. Nucleic Acids Res. *46* (D1), D1027–D1030.

Flavell, S.W., Kim, T.K., Gray, J.M., Harmin, D.A., Hemberg, M., Hong, E.J., Markenscoff-Papadimitriou, E., Bear, D.M., and Greenberg, M.E. (2008). Genome-wide analysis of MEF2 transcriptional program reveals synaptic target genes and neuronal activity-dependent polyadenylation site selection. Neuron *60*, 1022–1038.

Fu, Y., Sun, Y., Li, Y., Li, J., Rao, X., Chen, C., and Xu, A. (2011). Differential genome-wide profiling of tandem 3′ UTRs among human breast cancer and normal cells by high-throughput sequencing. Genome Res. *21*, 741–747.

Goldman, M., Craft, B., Swatloski, T., Cline, M., Morozova, O., Diekhans, M., Haussler, D., and Zhu, J. (2015). The UCSC Cancer Genomics Browser: update 2015. Nucleic Acids Res. *43*, D812–D817.

Hao, Y.H., Doyle, J.M., Ramanathan, S., Gomez, T.S., Jia, D., Xu, M., Chen, Z.J., Billadeau, D.D., Rosen, M.K., and Potts, P.R. (2013). Regulation of WASH-dependent actin polymerization and protein trafficking by ubiquitination. Cell *152*, 1051–1064.

Hao, Y.H., Fountain, M.D., Jr., Fon Tacer, K., Xia, F., Bi, W., Kang, S.H., Patel, A., Rosenfeld, J.A., Le Caignec, C., Isidor, B., et al. (2015). USP7 acts as a molecular rheostat to promote WASH-dependent endosomal protein recycling and is mutated in a human neurodevelopmental disorder. Mol. Cell *59*, 956–969.

Hoffman, Y., Bublik, D.R., Ugalde, A.P., Elkon, R., Biniashvili, T., Agami, R., Oren, M., and Pilpel, Y. (2016). 3'UTR shortening potentiates microRNA-based repression of pro-differentiation genes in proliferating human cells. PLoS Genet. *12*, e1005879.

Hoque, M., Ji, Z., Zheng, D., Luo, W., Li, W., You, B., Park, J.Y., Yehia, G., and Tian, B. (2013). Analysis of alternative cleavage and polyadenylation by 3′ region extraction and deep sequencing. Nat. Methods *10*, 133–139.

Ji, Z., and Tian, B. (2009). Reprogramming of 3′ untranslated regions of mRNAs by alternative polyadenylation in generation of pluripotent stem cells from different cell types. PLoS ONE *4*, e8419.

Ji, Z., Lee, J.Y., Pan, Z., Jiang, B., and Tian, B. (2009). Progressive lengthening of 3′ untranslated regions of mRNAs by alternative polyadenylation during mouse embryonic development. Proc. Natl. Acad. Sci. USA *106*, 7028–7033.

Johnson, S.A., Cubberley, G., and Bentley, D.L. (2009). Cotranscriptional recruitment of the mRNA export factor Yra1 by direct interaction with the 3′ end processing factor Pcf11. Mol. Cell *33*, 215–226.

Kamieniarz-Gdula, K., Gdula, M.R., Panser, K., Nojima, T., Monks, J., Wiśniewski, J.R., Riepsaame, J., Brockdorff, N., Pauli, A., and Proudfoot, N.J. (2019). Selective roles of vertebrate PCF11 in premature and full-length transcript termination. Mol. Cell *74*, 158–172.e9.

Lee, A.K., and Potts, P.R. (2017). A comprehensive guide to the MAGE family of ubiquitin ligases. J. Mol. Biol. *429*, 1114–1142.

Li, W., You, B., Hoque, M., Zheng, D., Luo, W., Ji, Z., Park, J.Y., Gunderson, S.I., Kalsotra, A., Manley, J.L., and Tian, B. (2015). Systematic profiling of poly(A)+ transcripts modulated by core 3′ end processing and splicing factors reveals regulatory rules of alternative cleavage and polyadenylation. PLoS Genet. *11*, e1005166.

Li, W., Park, J.Y., Zheng, D., Hoque, M., Yehia, G., and Tian, B. (2016). Alternative cleavage and polyadenylation in spermatogenesis connects chromatin regulation with post-transcriptional control. BMC Biol. *14*, 6.

Lian, Y., Sang, M., Ding, C., Zhou, X., Fan, X., Xu, Y., Lü, W., and Shan, B. (2012). Expressions of MAGE-A10 and MAGE-A11 in breast cancers and their prognostic significance: a retrospective clinical study. J. Cancer Res. Clin. Oncol. *138*, 519–527.

Licatalosi, D.D., Geiger, G., Minet, M., Schroeder, S., Cilli, K., McNeil, J.B., and Bentley, D.L. (2002). Functional interaction of yeast pre-mRNA 3′ end processing factors with RNA polymerase II. Mol. Cell *9*, 1101–1111.

MacDonald, C.C. (2019). Tissue-specific mechanisms of alternative polyadenylation: Testis, brain, and beyond (2018 update). Wiley Interdiscip. Rev. RNA *10*, e1526.

MacDonald, C.C., and Redondo, J.L. (2002). Reexamining the polyadenylation signal: were we wrong about AAUAAA? Mol. Cell. Endocrinol. *190*, 1–8.

Mallon, B.S., and Macklin, W.B. (2002). Overexpression of the 3′-untranslated region of myelin proteolipid protein mRNA leads to reduced expression of endogenous proteolipid mRNA. Neurochem. Res. *27*, 1349–1360.

Martin, G., Gruber, A.R., Keller, W., and Zavolan, M. (2012). Genome-wide analysis of pre-mRNA 3′ end processing reveals a decisive role of human cleavage factor I in the regulation of 3′ UTR length. Cell Rep. *1*, 753–763.

Masamha, C.P., Xia, Z., Yang, J., Albrecht, T.R., Li, M., Shyu, A.B., Li, W., and Wagner, E.J. (2014). CFIm25 links alternative polyadenylation to glioblastoma tumour suppression. Nature *510*, 412–416.

Matoulkova, E., Michalova, E., Vojtesek, B., and Hrstka, R. (2012). The role of the 3′ untranslated region in post-transcriptional regulation of protein expression in mammalian cells. RNA Biol. *9*, 563–576.

Mayr, C., and Bartel, D.P. (2009). Widespread shortening of 3'UTRs by alternative cleavage and polyadenylation activates oncogenes in cancer cells. Cell *138*, 673–684.

McMahon, K.W., Hirsch, B.A., and MacDonald, C.C. (2006). Differences in polyadenylation site choice between somatic and male germ cells. BMC Mol. Biol. *7*, 35.

Meinhart, A., and Cramer, P. (2004). Recognition of RNA polymerase II carboxy-terminal domain by 3′-RNA-processing factors. Nature *430*, 223–226.

Mermelshtein, A., Gerson, A., Walfisch, S., Delgado, B., Shechter-Maor, G., Delgado, J., Fich, A., and Gheber, L. (2005). Expression of D-type cyclins in colon cancer and in cell lines from colon carcinomas. Br. J. Cancer *93*, 338–345.

Miura, P., Shenker, S., Andreu-Agullo, C., Westholm, J.O., and Lai, E.C. (2013). Widespread and extensive lengthening of 3′ UTRs in the mammalian brain. Genome Res. *23*, 812–825.

Narasimha, A.M., Kaulich, M., Shapiro, G.S., Choi, Y.J., Sicinski, P., and Dowdy, S.F. (2014). Cyclin D activates the Rb tumor suppressor by monophosphorylation. eLife *3*, e02872.

Newman, J.A., Cooper, C.D., Roos, A.K., Aitkenhead, H., Oppermann, U.C., Cho, H.J., Osman, R., and Gileadi, O. (2016). Structures of two melanoma-associated antigens suggest allosteric regulation of effector binding. PLoS ONE *11*, e0148762.

Niu, M., Cho, J.H., Kodali, K., Pagala, V., High, A.A., Wang, H., Wu, Z., Li, Y., Bi, W., Zhang, H., et al. (2017). Extensive peptide fractionation and y_1 ion-based interference detection method for enabling accurate quantification by isobaric labeling and mass spectrometry. Anal. Chem. *89*, 2956–2963.

O'Connor, H.F., Lyon, N., Leung, J.W., Agarwal, P., Swaim, C.D., Miller, K.M., and Huibregtse, J.M. (2015). Ubiquitin-activated interaction traps (UBAITs) identify E3 ligase binding partners. EMBO Rep. *16*, 1699–1712.

Ogorodnikov, A., Levin, M., Tattikota, S., Tokalov, S., Hoque, M., Scherzinger, D., Marini, F., Poetsch, A., Binder, H., Macher-Göppinger, S., et al. (2018). Transcriptome 3'end organization by PCF11 links alternative polyadenylation to formation and neuronal differentiation of neuroblastoma. Nat. Commun. *9*, 5331.

Pagala, V.R., High, A.A., Wang, X., Tan, H., Kodali, K., Mishra, A., Kavdia, K., Xu, Y., Wu, Z., and Peng, J. (2015). Quantitative protein analysis by mass spectrometry. Methods Mol. Biol. *1278*, 281–305.

Panwar, B., Omenn, G.S., and Guan, Y. (2017). miRmine: a database of human miRNA expression profiles. Bioinformatics *33*, 1554–1560.

Park, H.J., Ji, P., Kim, S., Xia, Z., Rodriguez, B., Li, L., Su, J., Chen, K., Masamha, C.P., Baillat, D., et al. (2018). 3′ UTR shortening represses tumor-suppressor genes in trans by disrupting ceRNA crosstalk. Nat. Genet. *50*, 783–789.

Pineda, C.T., Ramanathan, S., Fon Tacer, K., Weon, J.L., Potts, M.B., Ou, Y.H., White, M.A., and Potts, P.R. (2015). Degradation of AMPK by a cancer-specific ubiquitin ligase. Cell *160*, 715–728.

Quinlan, A.R., and Hall, I.M. (2010). BEDTools: a flexible suite of utilities for comparing genomic features. Bioinformatics *26*, 841–842.

Rosenwald, A., Wright, G., Wiestner, A., Chan, W.C., Connors, J.M., Campo, E., Gascoyne, R.D., Grogan, T.M., Muller-Hermelink, H.K., Smeland, E.B., et al. (2003). The proliferation gene expression signature is a quantitative integrator of oncogenic events that predicts survival in mantle cell lymphoma. Cancer Cell *3*, 185–197.

Rutnam, Z.J., and Yang, B.B. (2012). The non-coding 3′ UTR of CD44 induces metastasis by regulating extracellular matrix functions. J. Cell Sci. *125*, 2075–2085.

Salmena, L., Poliseno, L., Tay, Y., Kats, L., and Pandolfi, P.P. (2011). A ceRNA hypothesis: the Rosetta Stone of a hidden RNA language? Cell *146*, 353–358.

Sandberg, R., Neilson, J.R., Sarma, A., Sharp, P.A., and Burge, C.B. (2008). Proliferating cells express mRNAs with shortened 3′ untranslated regions and fewer microRNA target sites. Science *320*, 1643–1647.

Sartini, B.L., Wang, H., Wang, W., Millette, C.F., and Kilpatrick, D.L. (2008). Pre-messenger RNA cleavage factor I (CFIm): potential role in alternative polyadenylation during spermatogenesis. Biol. Reprod. *78*, 472–482.

Sherr, C.J. (1995). D-type cyclins. Trends Biochem. Sci. *20*, 187–190.

Shi, Y., Di Giammartino, D.C., Taylor, D., Sarkeshik, A., Rice, W.J., Yates, J.R., 3rd, Frank, J., and Manley, J.L. (2009). Molecular architecture of the human pre-mRNA 3′ processing complex. Mol. Cell *33*, 365–376.

Sicinski, P., Donaher, J.L., Geng, Y., Parker, S.B., Gardner, H., Park, M.Y., Robker, R.L., Richards, J.S., McGinnis, L.K., Biggers, J.D., et al. (1996). Cyclin D2 is an FSH-responsive gene involved in gonadal cell proliferation and oncogenesis. Nature *384*, 470–474.

Simpson, A.J., Caballero, O.L., Jungbluth, A., Chen, Y.T., and Old, L.J. (2005). Cancer/testis antigens, gametogenesis and cancer. Nat. Rev. Cancer *5*, 615–625.

Su, S., Minges, J.T., Grossman, G., Blackwelder, A.J., Mohler, J.L., and Wilson, E.M. (2013). Proto-oncogene activity of melanoma antigen-A11 (MAGE-A11) regulates retinoblastoma-related p107 and E2F1 proteins. J. Biol. Chem. *288*, 24809–24824.

Takagaki, Y., and Manley, J.L. (1998). Levels of polyadenylation factor CstF-64 control IgM heavy chain mRNA accumulation and other events associated with B cell differentiation. Mol. Cell *2*, 761–771.

Takano, Y., Kato, Y., Masuda, M., Ohshima, Y., and Okayasu, I. (1999). Cyclin D2, but not cyclin D1, overexpression closely correlates with gastric cancer progression and prognosis. J. Pathol. *189*, 194–200.

Takano, Y., Kato, Y., van Diest, P.J., Masuda, M., Mitomi, H., and Okayasu, I. (2000). Cyclin D2 overexpression and lack of p27 correlate positively and cyclin E inversely with a poor prognosis in gastric cancer cases. Am. J. Pathol. *156*, 585–594.

Tian, B., and Manley, J.L. (2017). Alternative polyadenylation of mRNA precursors. Nat. Rev. Mol. Cell Biol. *18*, 18–30.

Volanakis, A., Kamieniarz-Gdula, K., Schlackow, M., and Proudfoot, N.J. (2017). WNK1 kinase and the termination factor PCF11 connect nuclear mRNA export with transcription. Genes Dev. *31*, 2175–2185.

Wang, X., Li, Y., Wu, Z., Wang, H., Tan, H., and Peng, J. (2014). JUMP: a tag-based database search tool for peptide identification with high sensitivity and accuracy. Mol. Cell. Proteomics *13*, 3663–3673.

Wang, R., Nambiar, R., Zheng, D., and Tian, B. (2018). PolyA_DB 3 catalogs cleavage and polyadenylation sites identified by deep sequencing in multiple genomes. Nucleic Acids Res. *46* (D1), D315–D319.

Weon, J.L., and Potts, P.R. (2015). The MAGE protein family and cancer. Curr. Opin. Cell Biol. *37*, 1–8.

Weon, J.L., Yang, S.W., and Potts, P.R. (2018). Cytosolic iron-sulfur assembly is evolutionarily tuned by a cancer-amplified ubiquitin ligase. Mol. Cell *69*, 113–125.e6.

Xia, L.P., Xu, M., Chen, Y., and Shao, W.W. (2013). Expression of MAGE-A11 in breast cancer tissues and its effects on the proliferation of breast cancer cells. Mol. Med. Rep. *7*, 254–258.

Xia, Z., Donehower, L.A., Cooper, T.A., Neilson, J.R., Wheeler, D.A., Wagner, E.J., and Li, W. (2014). Dynamic analyses of alternative polyadenylation from RNA-seq reveal a 3′-UTR landscape across seven tumour types. Nat. Commun. *5*, 5274.

Yao, C., Biesinger, J., Wan, J., Weng, L., Xing, Y., Xie, X., and Shi, Y. (2012). Transcriptome-wide analyses of CstF64-RNA interactions in global regulation of mRNA alternative polyadenylation. Proc. Natl. Acad. Sci. USA *109*, 18773–18778.

Ye, C., Long, Y., Ji, G., Li, Q.Q., and Wu, X. (2018). APAtrap: identification and quantification of alternative polyadenylation sites from RNA-seq data. Bioinformatics *34*, 1841–1849.

Yoon, J.H., and Gorospe, M. (2016). Cross-linking immunoprecipitation and qPCR (CLIP-qPCR) analysis to map interactions between long noncoding RNAs and RNA-binding proteins. Methods Mol. Biol. *1402*, 11–17.

Zhu, Y., Wang, X., Forouzmand, E., Jeong, J., Qiao, F., Sowd, G.A., Engelman, A.N., Xie, X., Hertel, K.J., and Shi, Y. (2018). Molecular mechanisms for CFIm-mediated regulation of mRNA alternative polyadenylation. Mol. Cell *69*, 62–74.e4.

STAR★METHODS

KEY RESOURCES TABLE

REAGENT or RESOURCE	SOURCE	IDENTIFIER
Antibodies		
Rabbit polyclonal anti-MAGE-A11	This paper	N/A
Rabbit polyclonal anti-PCF11	Bethyl Laboratories	Cat# A303-706A; RRID:AB_11204946
Rabbit polyclonal anti-RNAP II	Cell Signaling Technology	Cat# 14958; RRID:AB_2687876
Rabbit monoclonal anti- anti-CLP1	Abcam	N/A
Rabbit monoclonal anti- anti-HUWE1	Novus Biologicals	Cat# NB100-652; RRID:AB_2264587
Rabbit monoclonal anti-GAPDH	Cell Signaling Technology	Cat# 2118; RRID:AB_561053
Mouse monoclonal anti-FLAG	Sigma-Aldrich	Cat# F3165; RRID:AB_259529
Rabbit polyclonal anti-Myc	Sigma-Aldrich	Cat# C3956; RRID:AB_439680
Mouse monoclonal anti-Actin	Abcam	Cat# ab6276; RRID:AB_2223210
Mouse monoclonal anti-Tubulin	Sigma-Aldrich	Cat# T5168; RRID:AB_477579
Rabbit polyclonal anti-CCND1	ABclonal	Cat# A11022; RRID:AB_2758370
Rabbit polyclonal anti-CCND2	ABclonal	Cat# A1773; RRID:AB_2763815
Rabbit polyclonal anti-CCND3	ABclonal	Cat# A0746; RRID:AB_2757375
Rabbit polyclonal anti-phospho-Rb S807/811	Cell Signaling Technology	Cat# 9308; RRID:AB_331472
Mouse monoclonal anti-Rb	Cell Signaling Technology	Cat# 9309; RRID:AB_823629
Rabbit polyclonal anti-PTEN	Bethyl Laboratories	Cat# A300-701A; RRID:AB_2174186
Rabbit monoclonal anti-phospho-Akt T308	Cell Signaling Technology	Cat# 4056; RRID:AB_331163
Rabbit monoclonal anti-Akt	Cell Signaling Technology	Cat# 4691; RRID:AB_915783
Rabbit polyclonal anti-CPSF160	Bethyl Laboratories	Cat# A301-580A; RRID:AB_1078859
Rabbit polyclonal anti-CPSF100	Thermo Fisher Scientific	Cat# A301-581A; RRID:AB_1078861
Rabbit polyclonal anti-CPSF73	Bethyl Laboratories	Cat# A301-091A; RRID:AB_2084528
Rabbit polyclonal anti-CSTF64	Bethyl Laboratories	Cat# A301-092A; RRID:AB_873014
Rabbit anti-TauCSTF64	Bethyl Laboratories	Cat# A301-487A; RRID:AB_999545
Rabbit polyclonal anti-CPSF68	Bethyl Laboratories	Cat# A301-356A; RRID:AB_937781
Rabbit polyclonal anti-CPSF59	Bethyl Laboratories	Cat# A301-359A; RRID:AB_937869
Mouse monoclonal anti-NUDT21	Proteintech	Cat# 66335-1-Ig; RRID: N/A
Rabbit anti-XRN2	Bethyl Laboratories	Cat# A301-103A; RRID:AB_2218876
Mouse IgG control	Santa Cruz Biotechnology	Cat# sc-2025; RRID:AB_737182
Donkey Anti-Rabbit IgG, HRP Conjugated	GE Healthcare	Cat# NA934; RRID:AB_772206
Sheep Anti-Mouse IgG, HRP Conjugated	GE Healthcare	Cat# NA931; RRID:AB_772210
Bacterial and Virus Strains		
DH5a Competent Cells	Thermo Fisher Scientific	Cat# 18265017
XL1-blue Competent Cells	Agilent Technologies	Cat# 200130
One shot Stbl3	Life Technologies	Cat# C7373-03
BL21-codon plus(DE3)-RILP	Agilent Technologies	Cat# 230280
Chemicals, Peptides, and Recombinant Proteins		
ECL detection reagent	GE Healthcare	Cat# RPN2209
ECL prime detection reagent	GE Healthcare	Cat# RPN2236
Protein A beads	Bio-Rad	Cat# 1560005
Protein G Agarose	Thermo Fisher Scientific	Cat# 20389
Protein A/G PLUS agarose	Santa Cruz Biotechnology	Cat# sc-2003
Anti-FLAG M2 Beads	Sigma	Cat# A2220

(*Continued on next page*)

Continued

REAGENT or RESOURCE	SOURCE	IDENTIFIER
TUBE2-Agarose	LifeSensors	Cat# UM402
Effectene transfection reagent	QIAGEN	Cat# 301425
Lipofectamine RNAiMAX	Thermo Fisher Scientific	Cat# 13778030
Lipofectamine 2000	Invitrogen	Cat# 11668027
RNAStat60	TelTest	Cat# Cs-112
RNeasy Kit	QIAGEN	Cat# 74104
TEV Protease	Sigma-Aldrich	Cat# T4455
Calmodulin-Sepharose 4B	GE Healthcare	Cat# 17-0529-01
Glutathione Sepharose 4B	GE Healthcare	Cat# 17-0756-05
Critical Commercial Assays		
High Capacity cDNA Reverse Transcription kit	Thermo Fisher Scientific	Cat# 4368813
TNT SP6 Quick *In Vitro* TNT Kit	Promega	Cat# L2080
BCA protein assay kit	Thermo Fisher Scientific	Cat# 23227
AlamarBlue® Cell Viability Reagent	Thermo Fisher Scientific	Cat# DAL1100
Experimental Models: Cell Lines		
HEK293	ATCC	Cat# CRL-1573
HEK293T	Choe et al., 2016	N/A
HEK293T HUWE1 KO	Choe et al., 2016	N/A
HEK293FT	Thermo Fisher Scientific	Cat# R70007
A2780	A gift from Michael White, UT Southwestern	N/A
DAOY	ATCC	Cat# HTB-186
H520	A gift from John Minna UT Southwestern	N/A
OV56	A gift from Michael White, UT Southwestern	N/A
DAOY MAGE-A11 KO	This paper	N/A
H520 MAGE-A11 KO	This paper	N/A
Experimental Models: Organisms/Strains		
NOD.Cg-Prkdcscid Il2rgtm1Wjl/SzJ: NOD scid gamma mice	The Jackson Laboratory	005557; RRID: IMSR_JAX:005557
Oligonucleotides		
See Table S5	This paper	N/A
Software and Algorithms		
ImageJ software	ImageJ	https://imagej.nih.gov/ij
GraphPad Prism 7	GraphPad	https://www.graphpad.com
STAR version 2.5.2b	Dobin et al., 2013	https://github.com/alexdobin/STAR
DaPars	Xia et al., 2014	https://github.com/ZhengXia/dapars
MAT3UTR	Park et al., 2018	https://github.com/thejustpark/MAT3UTR
DESeq2	Anders and Huber, 2010	https://bioconductor.org/packages/release/bioc/html/DESeq2.html
HTSeq	Anders et al., 2015	https://htseq.readthedocs.io/en/release_0.11.1/count.html
Deposited Data		
Sequencing data	NCBI Gene Expression Omnibus	GEO: GSE134898
Proteomics data	MassIVE UCSD	MSV000084123

LEAD CONTACT AND MATERIALS AVAILABILITY

All materials generated in this study are available through request to Lead Contact Patrick Ryan Potts (ryan.potts@stjude.org).

EXPERIMENTAL MODEL AND SUBJECT DETAILS

Animals

6-8 week old male NOD.Cg-*Prkdc*^{scid} *Il2rg*^{tm1Wjl}/SzJ (NOD scid gamma) mice from Jackson Labs were used for xenograft growth assays. Animals were group housed under standard conditions. All studies were approved by the St. Jude Children's Research Hospital institutional review committee on animal safety.

Cell lines

HEK293FT, HEK293T, HEK293, A2780, and DAOY cells were grown in DMEM supplemented with 10% (v/v) FBS, 2 mM L-glutamine, 100 units/mL penicillin, 100 units/mL streptomycin, and 0.25 mg/mL amphotericin B. H520 cells were grown in RPMI supplemented with 5% (v/v) heat inactivated serum. OV56 cells were grown in DMEM:HAMS F12 (1:1) supplemented with 5% (v/v) FBS, 2 mM L-glutamine, 0.5 μg/mL hydrocortisone, and 10 μg/mL insulin. HEK293T HUWE1 knockout cells were described previously (Choe et al., 2016). Cell lines were authenticated by STR analysis. Sex of cells used: Female, HEK293FT, HEK293T, HEK293, A2780, OV56; Male, DAOY, H520. All cells were maintained at 37°C in 5% CO_2.

Microbe strains

DH5a (Thermo Fisher Scientific, #18265017) and XL1-blue (Agilent #200130) competent cells were used for standard molecular cloning and plasmid amplification. One shot Stbl3 competent cells (Life Technologies #C7373-03) were used for lentiviral plasmid cloning and plasmid amplification. BL21-codon plus (DE3)-RILP competent cells (Agilent Technologies, #230280) were used for recombinant protein production and purification. Bacteria were cultured under standard conditions at 37°C, 225 rpm.

METHOD DETAILS

Cell culture transfections

siRNA and plasmid transfections were performed using Lipofectamine RNAiMAX, Lipofectamine 2000 (Invitrogen) and Effectene (QIAGEN) according to the manufacturers' protocol.

Generation of stable overexpression cell lines

HEK293FT and DAOY cells were transfected with either HA-FLAG-vector or HA-FLAG-MAGE-A11 using Effectene according to the manufacturer's protocol in 6 cm^2 plates. After 48 hours, cells were selected with 1 μg/mL of puromycin over 2 weeks. HEK293 cells were transfected with either tandem affinity purification (TAP)-vector or TAP-MAGE-A11 using Effectene in 6 cm^2 plates. After 48 hours, cells were selected with 1 μg/mL of puromycin over 2 weeks. HEK293FT cells were transfected with TAP-MAGE-A11-UBAIT or TAP-MAGE-A11-UBAIT GG deletion using Effectene in 6 cm^2 plates. After 48 hours, cells were selected with 1 μg/mL of puromycin over 2 weeks. A2780, H520 and OV56 cells were transduced with Myc-vector or Myc-MAGE-A11 lentivirus using polybrene in 6-well plates. Two days after lentiviral transduction, cells were selected over 2 weeks using 2.5 μg/mL of blasticidin (GIBCO).

siRNA and miRNAs

siRNA transfections were performed using Lipofectamine RNAiMAX according to the manufacturer's protocol. All siRNAs were purchased from Sigma. siRNA targeting sequences; siControl, 5′-ACUACAUCGUGAUUCAAACUU; siMAGE-A11 #1, 5′- CAAGAU AAUUGAUUUGGUU; siMAGE-A11 #2, 5′-CUGAUAGACCCUGAGUCCU; siPCF11 #1, 5′-GUACCUUAUGGAUUCUAUU; siPCF11 #2, 5′- GUAUCUCACUGCCUUUACU; siPCF11 #3, 5′- CAACGUUAUGACAGUGUUA; siPCF11 #4, 5′-CAAUUGUUCCUGAUAU ACA. siCCND2 #1, 5′-CUCAUGACUUCAUUGAGCA; siCCND2 #2, 5′-CUGUGUGCCACCGACUUUA; siCCND2 #3, 5′-GAGGAAGU GAGCUCGCUCA; siHUWE1 #1, 5′- CAUGAGACAUCAGCCCACCCUUAAAA; siHUWE1 #2, and 5′- CACACCAGCAAUGGCUGC CAGAAUU. miRNA mimetics were purchased from Sigma. miRNA antagomirs were purchased from Applied Biological Materials Inc.

Antibodies

MAGE-A11 rabbit polyclonal antibody was generated against bacterially expressed MAGE-A11 (amino acids 197-429) (Cocalico Biologicals, Inc). Commercial antibodies used: anti-PCF11 (Bethyl Laboratories, A303-706A), anti-RNAP II (Cell Signaling Technology, 14958S), anti-CLP1 (Abcam, ab133669), anti-HUWE1 (Novus Biologicals, NB100-652), anti-GAPDH (Cell Signaling Technology, 2118S), anti-FLAG (Sigma, F3165), anti-Myc (Roche, 11666606001), anti-Actin (Abcam, ab6276), anti-Tubulin (Sigma, T5168), anti-CCND1 (ABclonal, A11022), anti-CCND2 (ABclonal, A1773), anti-CCND3 (ABclonal, A0746), anti-phospho-Rb S807/811 (Cell Signaling Technology, 9308T), anti-Rb (Cell Signaling Technology, 9309T), anti-PTEN (Bethyl Laboratories, A300-701A), anti-phospho-Akt T308 (Cell Signaling Technology, 4056S), anti-Akt (Cell Signaling Technology, 4691S), anti-CPSF160 (Bethyl Laboratories, A301-580A), anti-CPSF100 (Bethyl Laboratories, A301-581A), anti-CPSF73 (Bethyl Laboratories, A301-091A), anti-CstF64 (Bethyl Laboratories, A301-092A), anti-TauCstF64 (Bethyl Laboratories, A301-487A), anti-CFIm68 (Bethyl Laboratories, A301-356A), anti-CFIm59 (Bethyl Laboratories, A301-359A), anti-CFIm25 (Proteintech, 66335-1-Ig), anti-XRN2 (Bethyl Laboratories, A301-103A), Donkey anti-Rabbit IgG (GE, NA934V), and Sheep anti-Mouse IgG (GE, NA931V).

Tandem affinity purification

Ten 15 cm^2 plates of HEK293 cells stably expressing TAP-vector or TAP-MAGE-A11 were lysed with TAP lysis buffer (10% (v/v) glycerol, 50 mM HEPES-KOH pH 7.5, 100 mM KCl, 2 mM EDTA, 0.1% (v/v) NP-40, 10 mM NaF, 0.25 mM NA_3VO_4, 50 mM β-glyerolphosphate, 2 mM DTT, and 1X protease inhibitor cocktail) and cleared supernatants were bound to IgG-Sepharose beads (GE Amersham) and then washed in lysis buffer and TEV buffer (10 mM HEPES-KOH pH 8.0, 150 mM NaCl, 0.1% NP-40, 0.5 mM EDTA, 1 mM DTT, and 1X protease inhibitor cocktail). Protein complexes were cleaved off the beads by TEV protease and incubated with calmodulin-Sepharose beads (GE Amersham) in calmodulin binding buffer (10 mM HEPES-KOH pH 8.0, 150 mM NaCl, 1 mM Mg acetate, 1 mM imidazole, 0.1% NP-40, 6 mM $CaCl_2$, 10 mM 2-mercaptoethanol) and then washed, eluted with SDS sample buffer, subjected to SDS-PAGE, and stained with GelCode Blue stain (Thermo Fisher Scientific) before protein identification by LC-MS/MS.

RNA preparation and quantitative reverse transcription PCR Analysis (qRT-PCR)

RNA was extracted from cultured cells using RNAStat60 (TelTest) according to manufacturer's instructions. Total RNA was treated with DNase I (Roche) and converted to cDNA using High Capacity Reverse Transcription kit (Life Technologies). cDNA and appropriate primers were plated in triplicate in a 384-well plate and gene expression levels were measured using SYBR green master mix (Applied Biosystems). Oligonucleotides used for qRT-PCR: *MAGE-A11* forward, 5′-GAGGATCACTGGAGGAGAACA; reverse, 5′-TCTTTGCTCAAGAGGCATGAT; *CCND2* forward, 5′-TTCCCTCTGGCCATGAATTAC; reverse, 5′-GGGCTGGTCTCTTTGAGTTT; *CCND2* 3′-UTR forward #1, 5′-CTTCTGGTATCTGGCGTTCTT; reverse #1, 5′-CAGGCTTGTCTGAGGAATGT; *CCND2* 3′-UTR forward #2, 5′-GGACACCTTGTGTTTAGGATCA; reverse #2, 5′-GGGAGAAGGAAGCACCATAAA; *CCND2* 3′-UTR forward #3, 5′-CAAGCCTACCCGACTCTATTTAC; reverse #3, 5′-CCCAAGGATGGGAAAGAGAAA; *CCND2* 3′-UTR forward #4, 5′-TACTGGGT CATCCTTGGTCTAT; reverse #4, 5′-TTGTCTTCTCCTCTGGCTTTG.

Clonogenic growth and anchorage-independent growth soft agar assays

For clonogenic growth assays on plates, wild-type or knockout cells were plated in 6-well plates in triplicate. After 2-3 weeks, cells were fixed and stained with 0.05% (w/v) crystal violet and counted. For anchorage-independent growth soft agar assays, cells were suspended in 0.375% Noble agar (Difco) supplemented with regular growth medium and overlaid on 0.5% Noble agar. Cells were incubated for 2-4 weeks before colonies $\geq$ 100 μm in size were counted.

Immunoprecipitation and immunoblotting

HEK293FT cells were plated in 6 cm^2 plates and transfected 24 hours later with Effectene (QIAGEN) according to the manufacturer's protocol. After 48 hours, cells were washed and scraped in cold PBS, spun down, and resuspended in lysis buffer (50 mM Tris pH 7.4, 150 mM NaCl, 1 mM DTT, 0.1% (v/v) Triton X-100, 10 mM N-Ethylmaleimide (NEM), and 1X protease inhibitor cocktail). Cell lysates were incubated with appropriate antibodies overnight at 4°C and then with protein A beads for 2 hours at 4°C. Beads were then washed with lysis buffer three times and eluted with 2X SDS sample buffer. For immunoblotting, samples in SDS sample buffer were resolved on SDS-PAGE gels and then transferred to nitrocellulose membranes prior to blocking in TBST with 5% (w/v) milk powder or 3% (w/v) bovine serum albumin and probing with primary and secondary antibodies (GE Healthcare). Protein signal was visualized after addition of ECL detection reagent (GE Healthcare) according to manufacturer's instructions.

Recombinant protein purification and *in vitro* binding assay

GST-PCF11, GST-CLP1 or GST tag alone were induced in BL21 (DE3) cells at 16°C with isopropyl β-D-1-thiogalactopyranoside (IPTG). GST-tagged proteins were purified from bacterial lysates in lysis buffer (50 mM Tris pH 7.7, 150 mM KCl, 0.1% (v/v) Triton X-100, 1 mM DTT, 1 mg/mL lysozyme) with glutathione Sepharose (GE Amersham) and eluted with 10 mM glutathione. For *in vitro* binding assay, Myc-tagged proteins were *in vitro* translated using the SP6-TNT Quick rabbit reticulocyte lysate system (Promega) according to manufacturer's instructions. Purified GST-tagged proteins were bound to glutathione Sepharose beads for 1 hour in binding buffer (25 mM Tris pH 8.0, 2.7 mM KCl, 137 mM NaCl, 0.05% (v/v) Tween-20, and 10 mM 2-mercaptoethanol) and then were blocked for 1 hr in binding buffer containing 5% (w/v) milk powder. *In vitro* translated proteins were then incubated with the bound beads for 1 hour, washed, and the proteins were eluted in SDS-sample buffer, boiled, and subjected to SDS-PAGE and immunoblotting.

Tandem ubiquitin binding entity (TUBE) ubiquitination assay

HEK293FT, DAOY or H520 cells (1-2 10 cm^2 plates) were lysed with TUBE lysis buffer (50 mM Tris pH 7.5, 150 mM NaCl, 1 mM EDTA, 1% (v/v) NP-40, 10% (v/v) glycerol, 20 mM N-Ethylmaleimide (NEM), and 1X protease inhibitor cocktail), and the lysates were bound to TUBE-agarose (LifeSensors) overnight at 4°C. Beads were subsequently washed three times in wash buffer (20 mM Tris pH 8.0, 150 mM NaCl, 0.1% (v/v) Tween 20) and then the ubiquitinated proteins were eluted in SDS-sample buffer, boiled, and subjected to SDS-PAGE and immunoblotting.

Cell viability assay

To assess cell viability after siRNA knockdown, 1 X 10^4 cells/mL were transfected with 50 nM siRNA using Lipofectamine RNAiMAX according to the manufacturer's protocol and incubated for 72-96 hours prior to changing the media and adding alamarBlue (Thermo

Fisher Scientific) and incubating for 4 hours at 37°C. Plates were read by measuring the fluorescence with excitation wavelength at 540 nm and emission wavelength at 590 nm on an Enspire plate reader.

Xenograft tumor growth assays

3 X 10^6 DAOY wild-type and MAGE-A11 knockout cells were mixed with matrigel (Corning) before injection into the flank of NOD scid gamma mice (Jackson Lab) (n = 6 for wild-type group, n = 12 for MAGE-A11-knockout group). MAGE-A11 negative A2780 and OV56 ovarian cancer cells were made to stably express Myc-vector or Myc-MAGE-A11 before injection of 3 X 10^6 cells in PBS with matrigel into NOD scid gamma mice (n = 8 per group). Tumor size was measured 2-3 times a week during the duration of the experiment.

LightSwitch luciferase reporter assay

HEK293FT cells were seeded in a 96-well white plate (Corning Costar) in triplicate. After 24 hours, cells were transfected with 100 ng of LightSwitch luciferase reporter construct with PTEN 3′-UTR (SWTICHGEAR genomics) or 100 ng Renilla luciferase reporter using Lipofectamine 2000 according to the manufacturer's instructions and incubated for 24 hours. The luciferase assays were performed according to the manufacturer's protocol (SWTICHGEAR genomics).

RNA-seq

Total RNA was extracted from cultured cells or xenograft tumors using RNeasy kit (QIAGEN) according to manufacturer's instructions. RNA quality was assessed by 2100 Bioanalyzer RNA 6000 Nano assay (Agilent). Libraries were prepared using TruSeq Stranded mRNA kits (Illumina) and subjected to 100 cycle paired-end sequencing on the Illumina HiSeq platform.

CRISPR/Cas9 genome editing

Genetically modified cell lines were generated using CRISPR-Cas9 technology. Briefly, MAGEA11 KO DAOY cells were created by transiently co-transfecting 400,000 cells with 500 ng of each gRNA expression plasmid (cloned into Addgene plasmid #43860), 1 μg Cas9 expression plasmid (Addgene plasmid #43945), and 200 ng of pMaxGFP via nucleofection (Lonza, 4D-Nucleofector X-unit) using solution P3 and program EN-158 in small (20 μl) cuvettes according to the manufacturer's recommended protocol. MAGEA11 KO H520 cells were created by transiently co-transfecting 400,000 cells with 500 ng of each gRNA expression plasmid (cloned into Addgene plasmid #43860), 1 μg Cas9 expression plasmid (Addgene plasmid #43945), and 200ng of pMaxGFP via nucleofection (Lonza, 4D-Nucleofector X-unit) using solution P3 and program EH-100 in small (20 μl) cuvettes according to the manufacturer's recommended protocol. PCF11 I689A cells were created by transiently co-transfecting 400,000 cells with 500 ng of gRNA expression plasmid (cloned into Addgene plasmid #43860), 1 μg Cas9 expression plasmid (Addgene plasmid #43945), 2.1 μg of ssODN, and 200 ng of pMaxGFP via nucleofection (Lonza, 4D-Nucleofector X-unit) using solution P3 and program CA-137 in small (20 μl) cuvettes according to the manufacturer's recommended protocol. Five days post-nucleofection, cells were single-cell sorted by FACS to enrich for GFP+ (transfected) cells, clonally expanded and verified for the desired targeted modification via targeted deep sequencing followed by analysis using CRIS.py (Connelly and Pruett-Miller, 2019). Clones were identified for each modification and assessed in relevant assays. The sequences for genome editing reagents and applicable primers are listed below.

Name	Sequence (5′ to 3′)
hMAGEA11 KO reagents	
hMAGEA11.sgRNA.g1	GACGGCGGGACUAUGGGGGG
hMAGEA11.sgRNA.g2	UGUGGCCCUGAAGCAUGCAU
hMAGEA11.NGS.F partial Illumina adaptors (upper case)	CACTCTTTCCCTACACGACGCTCTTCCGATCTagcaaggctccctctctgctgtcag
hMAGEA11.NGS.R partial Illumina adaptors (upper case)	GTGACTGGAGTTCAGACGTGTGCTCTTCCGATCTtctccaagtcacccgatggaagaga
hPCF11 I689A reagents	
hPCF11 sgrna	CAGCUAUUUCAGUAUCAAGA
hPCF11 I689A ssODN I689A and blocking modifications (upper case)	agtgaacgtttagcatctggtgaaattacacaggatgacttccttgttgttgtgcatcaaGCtcgacagctattt caAtaCcaGgaaggtaaacatagatgcaatgtacgggatagtcctacagaagaaaataaaggtggatta
hPCF11.NGS.F partial Illumina adaptors (upper case)	CACTCTTTCCCTACACGACGCTCTTCCGATCTcccctatacagacgagtgaacg
hPCF11.NGS.R partial Illumina adaptors (upper case)	GTGACTGGAGTTCAGACGTGTGCTCTTCCGATCTtgaatgctgaacctgtgtcct

TCGA 3′-UTR analysis

The original TCGA RNA-seq gene expression data were obtained from the UCSC Cancer Genomics Hub (CGHub). All of the patients in a tumor type were ranked based on the CPM (count per million) values of *MAGE-A11* gene. The top 10 most highly MAGE-A11-expressed patients and bottom 10 least *MAGE-A11* expressed patients were chosen as two groups. The significant dynamics 3′-UTR usage genes between these two groups will be identified if the mean percentage of distal polyA usage (PDUI) change between

these two groups is larger than 0.2 and mean fold change is larger than 1.5, also the p value calculated from Student's t test is less than 0.05. Finally, we observed *MAGE-A11* promotes strong 3′-UTR shortening in two tumor types including ovarian cancer (OV) and lung squamous cell carcinoma (LUSC).

RNA-seq data analysis

RNA from cells with MAGE-A11 knocked out or overexpressed, and PCF mutant-expressing cells and controls were sequenced by HiSeq. The raw paired-end RNA-seq reads were filtering out low-quality reads using Trim Galore, and then aligned to the human genome (hg19/GRCh37) using STAR version 2.5.2b (Dobin et al., 2013) using the following alignment parameters: –outSAMtype BAM SortedByCoordinate –outSAMstrandField intronMotif –outFilterMultimapNmax 10 –outFilterMultimapScoreRange 1 –alignSJDBoverhangMin 1 –sjdbScore 2 –alignIntronMin 20 –alignSJoverhangMin 8. The resulted BAM files were converted into bedgraph format using bedtools version 2.17.0 (Quinlan and Hall, 2010). For each gene, the read count were calculated by HTSeq (Anders et al., 2015), and then CPM values based on read count were used. The read coverage was visualized at UCSC Genome Browsers (Goldman et al., 2015). Differential gene analysis was performed using DESeq2 (Anders and Huber, 2010).

DaPars analysis

DaPars (Feng et al., 2018; Xia et al., 2014) was used to identify the most significant APA events between two conditions. We require that significant APA events should meet three criteria. First, the adjusted p value of PDUI differences was controlled at 5%. Second, the absolute mean difference of PDUI must be no less than 0.2. Third, the mean PDUI fold change must be no less than 1.5.

CFIm25 motif analysis

MAGE-A11 sensitive transcripts were defined as those transcripts with significant 3′-US upon MAGE-A11 overexpression, while MAGE-A11 insensitive transcripts were an equal number of randomly selected unaffected transcripts (PDUI differences less than 0.05; p value larger than 0.5). For each DaPars predicted PAS, the nearest annotated PAS was defined as the true PAS. The annotated PASs were compiled from multiple domains including Refseq, ENSEMBL, UCSC gene models and PolyA_DB version 3 (Wang et al., 2018) databases. The sequences of 200 nucleotides upstream and downstream of the PASs were used for motif analysis. The CFIm25 motif density was calculated by counting the number of UGUA motif (smoothed over 7 nucleotide) along these specified annotation features, which included proximal and distal PAS.

CLIP-qPCR

Cross-linking immunoprecipitation and QPCR (CLIP-QPCR) was carried out as previously described (Yoon and Gorospe, 2016). Briefly, HEK293FT/HA-FLAG-Vector or HEK293FT/HA-FLAG-MAGE-A11 cells (10 15 cm^2 dishes) were washed in ice-cold, magnesium-free PBS and irradiated on ice with 150 mJ/cm^2 of UVC (254 nm) in a Stratalinker 2400 (Agilent). Cells were collected in ice-cold PBS, pelleted, lysed in NP-40 lysis buffer (50 mM Tris-HCl pH 7.5, 150 mM KCl, 0.5% (v/v) NP-40), and centrifuged for 15 min at 10,000 xg at 4°C. Supernatants were collected and subjected to immunoprecipitation. Cell lysates were incubated with 20 μL pre-coupled antibody-protein A/G PLUS-agarose beads (Santa Cruz Biotechnology) for 3 hr at 4°C rotating. Antibodies (10 μg) used were as follows: normal mouse IgG control (Santa Cruz, sc-2025) and anti-CFIm25 (Proteintech, 66335-1-Ig). Beads were then washed three times in NP-40 lysis buffer, treated with 20 units of RNase-free DNase I for 15 min at 37°C, and proteins degraded by treatment with 0.5 mg/mL proteinase K (Invitrogen) in 0.5% SDS at 55°C for 15 min. RNA was then separated by phenol: chloroform extraction, followed by ethanol precipitation. RNA was then converted to cDNA using the High Capacity cDNA reverse transcriptase kit (Invitrogen) according to manufacturer's instructions. qPCR analysis was performed on cDNA using PowerUp SYBR Green master mix (Applied Biosystems) according to manufacturer's instructions using the following primers: *CCND2* forward, 5′-TTCCCTCTGGCCATGAATTAC; reverse, 5′-GGGCTGGTCTCTTTGAGTTT and *RPLP0* forward 5′-TCTACAACCCTGAAGTGCTT GAT-3′, *RPLP0* reverse 5′-CAATCTGCAGACAGACACTGG-3′. Data were analyzed by ΔΔCt method normalizing to *RPLP0* and control normal IgG pulldowns.

Trans-effect analysis of 3′-US

We used MAT3UTR (Park et al., 2018) for the detection of trans-effect of MAGEA11-induced 3′-UTR shortening in ceRNA in two tumor types OV and LUSC. The Briefly, MAT3UTR can predict ceRNA partner expression changes by using its 3′-UTR shortening gene expression, 3′-UTR shortening gene level, microRNA binding sites and miRNA expression. The miRNA binding sites were compiled from a collection of TarBase, miRecords, miRTarBase and predicted miRNA-binding sites from TargetScanHuman version 6.2. Exon and CDS annotation for TCGA and miRNA expression were downloaded from Xena UCSC Genome browsers. The enrichment of ceRNA partner genes with tumor suppressor gene (TSG) and oncogene (OG) was calculated by fisher exact test. The annotation of TSG and OG were from TUSON prediction (Davoli et al., 2013) with top 500 genes ($p < 0.01$) selected.

Mass spectrometry analysis

Protein samples were digested and the resulting peptides were analyzed by an optimized LC-MS/MS platform (Pagala et al., 2015). For quantitative TMT analysis, the digested peptides were labeled with individual TMT reagents, equally pooled, and fractioned by basic pH reversed phase LC chromatography. Each fraction was then analyzed using acidic pH reverse phase nanoscale LC-MS/MS

(Bai et al., 2017). The collected MS data were processed for protein identification and quantification by database search using the JUMP software suite (Wang et al., 2014).

DATA AND CODE AVAILABILITY

Proteomics data are available at MassIVE MSV000084123. RNA-seq data are available at NCBI GEO: GSE134898.